(NASA-CR-177109) TURBULENT BOUNDARY LAYERS IN OSCILLATING FLOWS. PART 1: AN EXPERIMENTAL AND COMPUTATIONAL STUDY Final Technical Report, 1 Jun. 1982 - 31 Aug. 1985 (Iowa State Univ. of Science and Technology)

N86-29149

Unclas

G3/34 43241

College of Engineering

Iowa State University

TURBULENT BOUNDARY LAYERS IN OSCILLATING FLOWS:

AN EXPERIMENTAL AND COMPUTATIONAL STUDY

William J. Cook

February 10, 1986

ISU-ERI-Ames-86434

Final Technical Report (Part 1 of 2 parts)* for Grant NCC 2-200
entitled "Study of Turbulent Boundary Layers in Oscillating Flows"

Grant Period: June 1, 1982 to August 31, 1985

William J. Cook, Principal Investigator

J. D. Murphy, Grant Technical Monitor, NASA Ames Research Center, Moffett Field, CA

*Part 2: Giddings, T. A. and Cook, W. J., "Response of Hot Element Flush Wall Gauges in Oscillating Flow," ISU-ERI-Ames-86435, February, 1986.

engineering research institute

iowa state university COLLEGE OF ENGINEERING, AMES, IOWA 50011

ABSTRACT

An experimental-computational study of the behavior of turbulent boundary layers for oscillating air flows over a plane surface with a small favorable mean pressure gradient is described. Experimental studies were conducted for boundary layers generated on the test section wall of a facility that produces a flow with a mean free stream velocity and a superposed nearly-pure sinusoidal component over a wide range of frequency. Flows at a nominal mean free stream velocity of 50 m/s were studied at atmospheric pressure and temperature at selected axial positions over a 2 m test length for frequencies ranging from 4 to 29 Hz. Quantitative experimental results are presented for unsteady velocity profiles and longitudinal turbulence levels obtained from hot wire anemometer measurements at three axial positions. Mean velocity profiles for oscillating flows were found to exhibit only small deviations from corresponding steady flow profiles, while amplitudes and phase relationships exhibited a strong dependence on axial position and frequency. Since sinusoidal flows could be generated over a wide range of frequency, studies at fixed values of reduced frequency at different axial positions were studied. Results show that there is some utility in the use of reduced frequency to correlate unsteady velocity results. The turbulence level u'_{rms} was observed to vary essentially sinusoidally around values close to those measured in steady flow. However, the amplitude of oscillation and phase relations for turbulence level were found to be strongly frequency dependent. Numerical predictions were obtained using an unsteady boundary layer computational code and the Cebeci-Smith and Glushko turbulence models. Predicted quantities related to unsteady velocity profiles exhibit fair agreement with experiment when the Cebeci-Smith turbulence model is used.

1. INTRODUCTION

The behavior of turbulent boundary layers subjected to time-dependent free stream flows is of fundamental interest in several areas of fluid dynamics. Examples are those related to dynamic stall and buffeting that occur under certain conditions in the flow over helicopter rotor blades and blades in turbomachines. A number of experiments have been performed in recent years to study the behavior of turbulent boundary layers for flows with a periodic variation in free stream velocity. In parallel, theoreticians have worked to develop flow models and computational codes to predict the behavior of unsteady boundary layers. A number of these studies have been directed toward turbulent boundary layers developed on plane surfaces in essentially zero-mean-pressure-gradient flows as a first step in dealing with more complex flows. In the present investigation a joint experimental-computational study of the response of turbulent boundary layers for oscillating flows over a plane surface was performed. The purpose of this paper is first to describe the experimental study and the computational method and second to present comparisons of experimental results and predicted behavior for representative cases. Observations related to the comparisons are made.

The concept of ensemble-averaging (Telionis, 1981) provides the basis for experimental and theoretical treatment of the periodic turbulent boundary layer flows addressed here. The instantaneous value of a flow variable q at a fixed position in a periodic turbulent flow may be written as

$$\hat{q}(t) = q_m + \tilde{q}(t) + q'(t)$$

where q_m is the time average or mean value of q, $\tilde{q}(t)$ is the periodic component, and $q'(t)$ is the turbulent fluctuation. The ensemble average of

$\hat{q}(t)$ is defined as

$$q(t) = q_m + \tilde{q}(t)$$

where

$$q_m = \frac{1}{T}\int_0^T q(t)dt$$

$q(t)$ is a function defined by J values of q each of which is given by

$$q(t_i) = \frac{1}{N}\sum_{n=1}^{N} q[t_i + (n-1)\gamma]$$

In the above equation, γ is the period of the free stream oscillation, N is the number of cycles over which the average is obtained, and $t_i = (i/J)\gamma$, $i = 1,\ldots,J$.

The ensemble-averaged description of the free stream velocity in an oscillating flow with a sinusoidal variation for U(t) is, at a fixed position in the flow direction,

$$U(t) = U_m + U_1 \text{Cos } \omega t \qquad (1.1)$$

and ensemble-averaged velocity in the boundary layer is

$$u(y,t) = u_m(y) + \tilde{u}(y,t) = u_m(y) + u_1(y)\text{Cos}[\omega t + \phi(y)] \qquad (1.2)$$

where the subscript 1 denotes the half amplitude of the velocity oscillation, ω is the angular frequency, and ϕ is a phase angle. The ratio u_1/U_1 may exceed unity in the boundary layer and ϕ may exhibit both positive and negative values.

2. EXPERIMENTAL FACILITY

2.1 Facility Description

A number of experimental facilities have been used to study unsteady turbulent boundary layers in oscillating flows with zero or essentially zero mean pressure gradients. A review of facilities used in oscillating flow studies has been prepared by Carr (1981). Some of the facilities used by other investigators with air as the test medium in zero-mean-pressure

gradient flows will be briefly discussed. The first significant study of turbulent boundary layers is oscillating flows was performed by Karlsson (1959), and was carried out using an oscillating flow facility consisting of an upstream blower, screens, a contraction section, and a test section of rectangular cross section. The boundary layer generated on the test section wall was studied. Rotating vanes installed near the test section exit generated oscillating flow in the test section. Variations of this flow-generating technique have been used by others including Simpson, et al (1981), and Cousteix, et al (1977). Other successful methods for generating oscillating flows in air have been employed by Brembati (1975), and Patel (1977). Brembati used a tunnel with a flexible test section wall that oscillated sinusoidally normal to the flow direction to create a variation in free stream velocity. Patel used a blower-driven contraction section that delivered flow to a horizontal test plate enclosed only by vertical walls. Flaps at the exit of the flow-delivery section were oscillated sinusoidally to induce travelling vortices in the flow over the test plate, thereby producing a unique type of oscillating flow. With the exception of Patel's facility, all of the above mentioned facilities produce oscillating flows that are relatively free of higher harmonics only when operated at a discrete frequency or, in some cases, at approximately twice the discrete frequency.

The facility developed in this study generates flows by a method that is conceptually quite different from those used in other studies. The facility is illustrated in Figure 1 and is further described in Table 1. It consists of an entrance section and a test section of square cross section and length L which is terminated by a convergent-divergent nozzle that has a two-dimensional contour. The nozzle discharge region pressure

is sufficiently low during testing to produce sonic flow at the nozzle throat. When the position of the wedge of the wave generator is fixed, the test section flow, which is subsonic, will be steady. When the wave generator mechanism is operated, the test section free stream flow at any x position is characterized by a non-zero mean velocity and a superposed oscillating component. The mechanism consists of a scotch yoke which imparts sinusoidal axial motion to the wedge when the input shaft is driven at constant speed. As the wedge undergoes motion, the sonic throat area varies, thereby varying the mass rate of flow and producing a wave pattern in the test section. The wave form developed depends on the contour of the wedge surface. A ramp-type symmetric wedge with a small leading-edge included angle produces an essentially pure sinusoidal velocity variation. For a given nozzle-wedge configuration, a change in wedge stroke produces a change in the amplitude of free stream velocity. Wedge strokes used during the course of this study are listed in Table 1.

The turbulent boundary layer studied in the present investigation was that generated on the test section wall. Boundary layer trip wires placed on all four walls at x = 0.13 m (Figure 1) were chosen to cause transition to occur at the trip location. The wire diameter to produce transition at the trip was determined by the method of Smith and Clutter (1959). The test section was square in cross section (7.5 cm x 7.5 cm) for its full length. As a result of boundary layer growth, a mild favorable pressure gradient existed in the flow. The origin of the wall boundary layer was taken at the trip location. The nominal mean test section velocity was 50 m/s. Thus the flow was in the incompressible regime.

The present technique for generating oscillating flows has the following advantages. First, the sonic throat isolates the test section

from downstream disturbances. A properly designed entrance section will deliver flow to the test section with a relatively low disturbance level. The result is a test section flow that has a minimum of extraneous disturbances. Second, with a ramp type wedge an essentially-pure sinusoidal free stream velocity variation can be produced over a wide range frequency. Third, independent changes in the mean flow velocity and the amplitude of oscillation can be made with relative ease by changing the configuration of the nozzle throat and the wedge of the wave generator. Flows with large amplitudes of oscillation can be generated. Fourth, due to the manner in which the flow is generated, an analytical description of the mainstream flow can be obtained. An accurate description of the mainstream velocity distribution with position and time is required for theoretical analysis of the boundary layer behavior. The following is the development of this description.

2.2 Analytical Description of Free Stream Flow

The oscillating free stream flow is assumed to be isentropic and effects of the wall boundary layer are ignored. Thus the flow is described in terms of the space coordinate x (Figure 1) and time. Under these conditions the free stream velocity in the test section is

$$U(x,t) = U_m + \tilde{U}(x,t)$$

The analysis presented here is for small amplitudes of oscillation. Therefore, the amplitude of the varying component $\tilde{U}(x,t)$ is assumed to be small compared to the mean value U_m. The governing equation for the velocity variation that develops in the test section under these conditions is the wave equation in the form

$$(a_m^2 - U_m^2)\Phi_{xx} - 2U_m\Phi_{xt} - \Phi_{tt} = 0 \tag{2.1}$$

where Φ is the velocity potential function, which is related to $\tilde{U}(x,t)$ by

$$\tilde{U}(x,t) = \partial\Phi(x,t)/\partial x$$

Solutions to equation (2.1) have been obtained in this study for sinusoidal $\tilde{U}(x,t)$. For reasons related to boundary conditions for equation (2.1) the solution will be written in terms of the Mach number $M(x,t) = U(x,t)/a_m$ where a_m is the mean acoustic velocity. The Mach number in the test section is

$$M(x,t) = M_m + \tilde{M}(x,t)$$

$$= M_m - S(x)\mathrm{Cos}[\omega t + \Delta(x)] \qquad (2.2)$$

where ω is the wedge angular frequency, $S(x)$ is the half amplitude of the Mach number variation, and $\Delta(x)$ is a phase angle. The latter are given by

$$S(x) = [(B\mathrm{Cos}\kappa + C\mathrm{Cos}n\kappa)^2 + (B\mathrm{Sin}\kappa - C\mathrm{Sin}n\kappa)^2]^{1/2} \qquad (2.2a)$$

$$\Delta(x) = \tan^{-1}[\frac{B\mathrm{Sin}\kappa - C\mathrm{Sin}n\kappa}{B\mathrm{Cos}\kappa + C\mathrm{Cos}n\kappa}] \qquad (2.2b)$$

where

$$n = (1 - M_m)/(1 + M_m) \qquad (2.2c)$$

$$\kappa = (x\omega/a_m)/(1 - M_m) \qquad (2.2d)$$

and B and C are constants yet to be determined. The corresponding pressure in the test section is

$$P(x,t) = P_m + \tilde{P}(x,t)$$

where $P(x,t) = p(x,t)/kp_m$ is a dimensionless pressure. $p(x,t) = p_m + \tilde{p}(x,t)$ is the absolute pressure, k is the specific heat ratio C_p/C_v for the test gas (air in this study) and p_m is the mean pressure. The solution for the pressure is

$$P(x,t) = P_m + W(x)\mathrm{Cos}[\omega t + \psi(x)] \qquad (2.3)$$

in which

$$W(x) = [(B\mathrm{Cos}\kappa - C\mathrm{Cos}n\kappa)^2 + (B\mathrm{sin}\kappa + C\mathrm{Sin}n\kappa)^2]^{1/2} \qquad (2.3a)$$

and

$$\psi(x) = \tan^{-1}\left(\frac{B\mathrm{Sin}\kappa + C\mathrm{Sin}n\kappa}{B\mathrm{Coz}\kappa - C\mathrm{Cos}n\kappa}\right) \qquad (2.3b)$$

For a specified value of the mean Mach number, equation (2.2c) yields n in equations (2.2a,b) and (2.3a,b). Additionally, equation (2.2d) relates κ to x when ω and a_m are specified. Equations (2.2) and (2.3) then yield the time and position dependent Mach number (velocity) and dimensionless pressure for the test section provided the constants B and C in equation (2.2a,b) and (2.3a,b) can be determined. Evaluation of these constants requires two boundary conditions. Assumptions related to these boundary conditions are that the entrance section flow and the flow in the converging section of the nozzle are isentropic and quasi-steady. These assumptions are appropriate if the entrance section and the converging section of the nozzle are short compared to the length of the test section. The first boundary condition is obtained at x = L. The ratio of the cross sectional area at the nozzle entrance, A_L, to the sonic are A^* changes with time as A^* changes due to the motion of the wedge. Imposing the assumption of isentropic quasi-steady flow in the converging section of the nozzle, M(L,t) is given implicitly by the relation between A/A^* and the Mach number for isentropic flow, which is

$$A_L/A^*(t) = [1/M(L,t)]\{[2/(k-1)] + [(k-1)/(k+1)][M(L,t)]^2\}^{(k+1)/[2(k-1)]} \qquad (2.4)$$

For small changes in A^* at low subsonic values of Mach number, M is nearly linear with A^*/A. Therefore, a sinusoidal variation in A^* for low Mach number flows will produce a variation in M(L,t) that is essentially sinusoidal. From equation (2.2) evaluated at x = L,

$$M(L,t) = M_m - S(L)\mathrm{Cos}[\omega t + \Delta(L)]$$

where $S(L) = S_L$ represents the half amplitude of the Mach number variation at x = L. M_m is found from the A/A^* - Mach number relation using A/A^*

determined with the wedge positioned at mid-stroke. Further, S_L depends only on the geometry of the wave generator, i.e., the nozzle throat cross sectional area, the wedge included angle, and the wedge stroke. Thus, for a specified configuration of the wave generator, the boundary condition at x = L yields one equation relating the constants B and C. This equation is obtained from equation (2.2a) as

$$S_L = [(B\text{Cos}\kappa_L + C\text{Cos}n\kappa_L)^2 + (B\sin\kappa_L - C\text{Sin}n\kappa_L)^2]^{1/2} \qquad (2.5)$$

The second boundary condition is related to the pressure variation at x = 0. Equations (2.3a) and (2.3b) evaluated at x = 0 yield

$$W(0) = W_o = B - C \qquad (2.6)$$
$$\psi(0) = 0$$

From equation (2.3) the pressure variation at x = 0 becomes

$$\tilde{P}(0,t) = W_o\text{Cos}\ \omega t \qquad (2.7)$$

Equation (2.6) provides the second relation between the constants B and C. From equations (2.5) and (2.6) the following expressions are obtained

$$B = [W_o + \{W_o^2 - 2(W_o^2 - S_L^2)/(1+z)\}^{1/2}]/2$$
$$C = B - W_o \qquad (2.8)$$

where

$$z = \text{Cos}\kappa_L\text{Cos}n\kappa_L - \text{Sin}\kappa_L\text{Sin}n\kappa_L$$

While S_L is known from specification of the wave generator geometry, W_o is unknown. Obtaining the value for W_o is related to the quasi-steady isentropic flow assumption for the entrance section. This assumption relates p(0,t) to M(0,t) through the relation

$$p(0,t)/p^o = \{1/[1+(k-1)(M^2(0,t)/2)]\}^{k/(k-1)} \qquad (2.9)$$

where p^o is the stagnation pressure of the air in the supply reservoir; the atmosphere in the present case. The expression

$$p(0,t)/p^o = p_m/p^o + \tilde{p}(0,t)/p^o$$

combined with equation (2.9) to form the dimensionless pressure variation at $x = 0$ yields

$$\tilde{P}(0,t) = \tilde{p}(0,t)/kp_m = (p^o/kp_m) \left[\left(\frac{1}{1+(k-1)(M^2(0,t)/2}\right)^{k/(k-1)} - p_m/p^o\right] \tag{2.10}$$

Equation (2.10) yields a periodic but not exactly sinusoidal $\tilde{P}(0,t)$ for a sinusoidal $M(0,t)$. Denoting $\tilde{P}'$ as the pressure variation obtained from equation (2.10), an equation similar in form to equation (2.7) can be written as

$$\tilde{P}'(0,t) = W_o' \mathrm{Cos}\,\omega t \tag{2.11}$$

where W_o' is the half amplitude of the pressure variation produced by equation (2.10). $M(0,t)$ for equation (2.10) is given by equation (2.2) as

$$\begin{aligned} M(0,t) &= M_m + \tilde{M}(0,t) = M_m - S(0)\mathrm{Cos}[\omega t + \Delta(0)] \\ &= M_m - S_o \mathrm{Cos}\,\omega t \end{aligned} \tag{2.12}$$

However, evaluation of S_o from equation (2.2a) requires values for B and C, which according to equations (2.8) depend on the known S_L and the unknown W_o. The solution is obtained through iteration by first guessing a value for W_o. This will yield values for B and C through equations (2.8). S_o is then found from equation (2.2a); $S_o = B + C$. Then substitution of $M(0,t)$ from equation (2.12) into equation (2.10) will then yield W_o' in equation (2.11), which is then compared with the guessed value of W_o. Iteration by means of a computer will result in $W_o' = W_o$ within a specified small tolerance, at which point values for B and C are established. These values then produce the analytical predictions for the Mach number (velocity) and pressure by means of equations (2.2) and (2.3). Comparisons of predicted and experimentally observed free stream flows are made subsequently.

3. DATA ACQUISITION SYSTEM

A hot wire anemometer system was used as the primary means of obtaining data. Figure 2 describes the data acquisition system used throughout this study. A DISA P14 single-wire probe mounted on a 4 mm diameter probe support was positioned through a wall of the test section. All data were taken at the half-height position on a vertical wall. The hot wire system was calibrated using a TSI model 1125 airflow calibrator, and the calibration was checked periodically during the experiments. During the course of this investigation several different hot wire probes were calibrated and used. The data acquisition system was used for both steady and unsteady flow measurements. For steady flow boundary surveys the system was programmed to read and process 500 hot wire voltage values at each probe position. For oscillating flow studies the system was programmed to read 20 hot wire voltage values at equally-spaced time intervals per cycle of flow oscillation and was triggered electronically once per revolution of the wave generator drive shaft. The shaft frequency was monitored by a photoelectric device. The system was programmed to take data for 210 cycles. Ensemble averaged velocities were obtained by processing the 210 hot wire voltage readings at each of the 20 points in the cycle. The data processing included the statistical fitting of a cosine wave to the 20 ensemble averaged values. The maximum data acquisition rate for the system was 1000 voltage readings per second. Data taken during this study were acquired at rates well below this value.

4. STEADY FLOW EXPERIMENTS

Detailed hot wire measurements were made at various x stations along the test section with the wave generator wedge locked at mid-stroke to provide a description of the test section flow under steady conditions.

Figure 3 presents as a function of test section axial position results for several flow quantities determined from the steady flow measurements. Due to the growth of the wall boundary layers there was a detectable increase with x of the steady centerline velocity U_s. The velocity increase described in Figure 3 corresponds to a measured pressure drop of 4.1 cm of water (0.40 kPa) over the test section length. Thus a mild favorable pressure gradient existed in the test section. Figure 3 also shows the test section centerline turbulence intensity u'_r/U_s vs x, where $u'_r = u'_{rms} = [\overline{u'^2}]^{1/2}$. These measurements were made by using a true rms meter and a 10 kHz low-pass filter in place of the voltmeter and the computer in the data acquisition system in Figure 2. The purpose of the filter was to eliminate high frequency electrical noise on the anemometer output signal that produced false readings at low turbulence levels. The turbulence intensity ranged from 0.1 percent at the test section entrance to 0.4 percent at x = 1.7 m.

Measured values for δ_s, the boundary layer velocity thickness for steady flow determined at 99 percent of the local centerline velocity, are also shown in Figure 3. The curve fitted through the data points indicates that the boundary layer grew according to the relation $\delta_s = 1.47\xi^{0.74}$, where δ_s is in cm and ξ is the distance in meters from the boundary layer trip wires (Figure 1). The boundary layer growth expression is consistent with the presence of a mild favorable pressure gradient. For zero pressure gradient turbulent flows, for which the accepted exponent is 0.8, a more rapid growth with ξ occurs.

The ratio of δ_s to the test section height h increases with ξ to a value of about 1/4 at the most down-stream measurement station, $\xi = 1.58$ m. The thickness of the wall boundary layer relative to the test section

height h is of concern in rectangular and square ducts since for sufficiently large values of δ/h secondary flows in the corners apparently cause cross flow in the boundary layer which destroys the nominally two dimensional boundary layer flow at mid plane. This matter has been studied experimentally and analytically by Brederode and Bradshaw (1978). It was found that the effect of secondary corner flows on the mid-plane boundary layer is negligible for $\delta/h \leq 1/4$, and that under this condition, the boundary layer flow on the wall at mid-plane in a square duct of constant cross section is quite close to that on a flat plate. Since the condition $\delta/h \leq 1/4$ is nominally met in the present study, flat-plate-like flows were expected on the test section side wall for $\xi \leq 1.58$ m.

Momentum thickness Reynolds numbers shown in Figure 3 for the boundary layer exceed 3600 for $x > 0.74$ m and indicate that a fully turbulent boundary layer was generated. The values shown for the boundary layer shape parameter $H = \delta^*/\theta$ are typical of those for a flat plate turbulent boundary layer in a zero pressure gradient flow. A small pressure gradient does not significantly influence H.

Figure 4 presents measured steady flow velocity profiles and turbulence intensity in terms of y/δ_s for three ξ stations; 0.61, 1.12, and 1.58 m. δ_s was taken as that given by the equation fitted to the experimental values of δ_s vs ξ in Figure 3. Figure 4a shows velocity profiles in terms of u/U_s and y/δ_s. The three profiles shown are in good agreement. Figure 4b shows steady boundary layer velocity profiles at the same three ξ stations in terms u^+ vs y^+ where $u^+ = u/u_\tau$, $u_\tau = (\tau_w/\rho)^{1/2}$, and $y^+ = u_\tau y/\nu$. τ_w was evaluated by the Ludwieg-Tillman law (Coles, 1968). The experimental results at 1.12 m and 1.58 m agreement at low values of y^+ with the logarithmic law region equation. A small difference exists

between the experimental and predicted results at $\xi = 0.61$ m.

Boundary layer turbulence intensities in terms of u'_r/u and y/δ_s are presented in Figure 4c for the three ξ stations. Turbulence intensities in the figure were determined by computer processing of the 500 hot-wire voltage values read using the data acquisition system in Figure 2 and, except at low values of turbulence intensity, were in agreement with readings obtained using the previously-mentioned 10 kHz low pass filter and rms voltmeter. As expected, the results at the three values of ξ collapse toward a single curve.

The collective results in Figures 3 and 4 indicate that a turbulent boundary layer typical of that developed in a flow with a mild favorable pressure gradient was produced in the test section under steady flow conditions.

5. OSCILLATING FLOW EXPERIMENTS

5.1 Free Stream Velocity Variation

As noted previously, the facility used in the present study produces an essentially-pure sinusoidal velocity variation in test section for a wide range of frequency. This is demonstrated in Figure 5 which shows velocity variations measured in the test section for two values of frequency at two positions using the data acquisition system described in Figure 2. The wave generator configuration described in Table 1 with a wedge stroke of 1.91 cm was used to produce the velocity variations shown in Figure 5. The symbols represent velocity values obtained by ensemble averaging velocity measurements (20 points per cycle) over 210 cycles. The curves are cosine waves fitted to the 20 ensemble averaged velocity values for the cycle. The three upper curves describe velocities measured in the free stream at two positions, ξ = 0.305 and 1.58 m, while the lower curve

is the velocity measured in the boundary layer at $y/\delta_s = 0.1$ at 1.58 m. It is evident in each case that the curve closely fits the data. Expressions for the fitted curves in the form of equations (1.1) and (1.2) permitted accurate evaluation of the mean velocities, amplitudes, and phase angles from the experimental data.

The two upper curves in Figure 5 demonstrate the effect of frequency on the free stream velocity variation at a fixed value of ξ. These curves are for velocity variations at $\xi = 1.58$ m. It is evident that the amplitude U_1 for the velocity at 29.4 Hz is larger than that for 15.5 Hz. Further, the velocity variation at 29.4 Hz leads that at 15.5 Hz by a small angle. The two free stream velocity curves in Figure 5 obtained at 15.5 Hz, one at $\xi = 0.305$ m and the other at $\xi = 1.58$ m, demonstrate the effect of position on the free stream velocity at a fixed frequency. Due to the increase in the mean free stream velocity in the direction of flow (as noted also for steady flow in Figure 3), the curve for $\xi = 1.58$ m at 15.5 Hz lies above that for $\xi = 0.305$ m in Figure 5. However, U_1 at $\xi = 1.58$ m is smaller than U_1 at 0.305 m. It is also evident from the figure that the free stream velocity at 1.58 m leads the velocity at 0.305 by a small angle.

The variation in the free stream velocity amplitude and phase angle with frequency and position can be predicted for a specified configuration of the wave generator by the analytical method previously outlined. For this analysis it is necessary to specify the mean Mach number M_m and the Mach number amplitude at x = L, S_L in equation (2.5). M_m can be found from equation (2.4) using $A(L)/A^*$ determined from the wave generator configuration with the wedge positioned at mid-stroke. The extremes of $A(L)/A^*$ can be determined from the wave generator configuration for a

specified wedge stroke, from which S_L can then be found using equation (2.4). Solutions for $S(x)$ and $\Delta(x)$, equations (2.2a) and (2.2b), can then obtained at the mean Mach number M_m. It may be difficult to accurately determine M_m and S_L from the wave generator configuration if small dimensions are involved. An alternate method for evaluating M_m and S_L involves measuring the free stream velocity in the test section with the wedge fixed at each of three positions; fully upstream, mid stroke, and fully downstream. From these measurements M_m and S_L can be accurately determined. Figure 6 shows solutions for $S(x)$ and $\Delta(x)$ at four values of frequency ranging from 1 to 29.4 Hz for the wave generator described in Table 1 at a wedge stroke of 1.91 cm. The values of M_m and S_L for the results in Figure 6 are 0.142 and 0.018 and were obtained using the alternate method from velocity measurements made at the test section half-length position. Also shown in Figure 6 are values of S and Δ obtained from velocity measurements in the free stream at three values of frequency at several x positions in the test section, i.e., from results like those for the free stream velocity in Figure 5. The agreement between the analytical solution and the experimental results is generally good. Both the experimental and analytical results indicate that the amplitude of oscillation departs from low frequency uniformity with x as frequency increases and that the phase angle exhibits a progressively increasing dependence on x as frequency increases. The results in Figure 6 demonstrate that both the free stream velocity variation and the phase angle variation with frequency and x can be predicted with reasonable accuracy by the analytical method.

5.2 Boundary Layer Velocity Variation

The major emphasis of the experimental phase of this investigation was

on acquiring data to describe the boundary layer behavior in oscillating flows. A total of twenty boundary layer surveys were conducted at four test section axial positions, $\xi = 0.61$, 0.91, 1.12, and 1.58 m, for frequencies ranging from 3.85 to 29.4 Hz using the data acquisition system described in Figure 2. Frequencies in this range are considerably below the estimated turbulent burst frequency, 500 Hz, obtained from the expression $U_m/5\delta_s$ (Rao, Naradinha, and Badri Narayanan, 1971). The results of each survey are denoted as a data set. Data set designations and conditions at which each was obtained are tabulated in Table 2. Conditions for the surveys were selected to provide results for comparisons at fixed values of position, frequency, and reduced frequency $\bar{\omega} = \omega\xi/U_m$. The range of reduced frequency covered by the surveys was 0.54 to 4.16. While $\bar{\omega}$ is a similarity variable for zero pressure gradient laminar oscillating boundary layers, exact similarity in terms of $\bar{\omega}$ for turbulent oscillating boundary layers does not exist (Telionis, 1981). Nonetheless, data were obtained at fixed values of $\bar{\omega}$ at several ξ stations in an attempt to assess the extent to which $\bar{\omega}$ serves as a correlating variable.

The amplitude of oscillation of the free stream velocity may have an influence on boundary layer behavior. It is evident from Figure 6 that the amplitude of velocity oscillation at high frequencies varies with position along the test section. The values for U_1/U_m listed in Table 2 were obtained from free stream velocity measurements at the location where the survey was conducted. U_1/U_m could be varied from survey to survey by changing the wedge stroke. The wedge stroke for each survey is listed in Table 2. There are four pairs of data sets for which conditions were identical or essentially identical within the pairs except for wedge stroke. These pairs of surveys were performed to assess the effect of

amplitude of velocity oscillation on results for a limited range of U_1/U_m.

Results for the oscillating flow boundary layer surveys will be presented in terms of the quantities in equations (1.1) and (1.2). Equation (1.2) represents the ensemble averaged velocity in the boundary layer produced by the free stream velocity variation described in equation (1.1). Descriptive quantities are u_m/U_m, the ratio of the mean boundary layer velocity to that in the free stream; u_1/U_1, the ratio of the half-amplitude of oscillation in the boundary layer to that in the free stream; and ϕ, the phase angle of the boundary layer velocity variation relative to that in the free stream. It is useful to present these quantities in terms of y/δ_s, where δ_s is the local boundary layer velocity thickness for steady flow as presented in Figure 3. Use of this ratio readily permits evaluation of the extent of unsteady effects in the y direction relative to the steady boundary layer thickness. Values for U_m and U_1 in the free stream and u_m, u_1, and ϕ in the boundary layer were determined from equations for the cosine curves fitted to ensemble averaged velocity data. A typical case is presented in Figure 5, in which the boundary layer velocity variation at $y/\delta_s = 0.10$ and the corresponding free stream velocity variation at $\xi = 1.58$ m and 15.5 Hz are shown. It is seen from the figure that the velocity variation in the boundary layer is essentially sinusoidal and that it leads the velocity variation in the free stream.

Figure 7 presents representative results for mean velocity profiles in terms of u_m/U_m and y/δ_s at three values of ξ. The oscillating flow data cover a wide range of frequency (see Table 2). Results of the steady flow velocity surveys are also shown in Figure 7. Estimates of uncertainties related to the velocity measurements indicate a small uncertainty region

about the size of the symbols. At $\xi \approx 0.61$ m, Figure 7a, the mean profiles for oscillating flow agree well with the steady flow profile. Results at $\xi \approx 1.12$ and 1.58 m, Figures 7b and 7c, show small differences in the unsteady and steady mean profiles, with the difference in Figure 7c the most noticeable.

Figures 8 and 9 present results for the amplitude ratio u_1/U_1 and the phase angle ϕ respectively at $\xi = 0.61$, 1.12, and 1.58 m in terms of y/δ_s for several values of frequency of oscillation. The results included in these figures were obtained for flows generated with the wedge stroke set at 1.91 cm, and, as noted in Table 2, values of U_1/U_m ranged from 0.121 to 0.239. Prior to discussion of these figures it is appropriate to consider the uncertainties of the results presented therein since these bear on conclusions drawn.

One of the sources of uncertainty in the oscillating flow results is related to the number of cycles over which the velocity measurements are ensemble averaged. Generally, due to the random nature of turbulence, ensemble averaging over a small number of cycles results in larger uncertainties for u_1 and ϕ than does averaging over a large number of cycles. In order to assess these uncertainties, the input to the data acquisition system (instantaneous readings of the oscillating flow velocity) was modeled using a digital computer and a statistical analysis was performed at various positions in the boundary layer for oscillating flows with ensemble averaged velocity variations, as described by equation (1.2), typical of those observed experimentally. The level of turbulence is an important parameter in the uncertainty analysis. In the free stream where u'_r, the rms turbulence level, is small compared to the amplitude of velocity oscillation U_1, an accurate representation of the ensemble

averaged velocity variation can be obtained by averaging over a relatively few cycles, while in the boundary layer, where u'_r may be near u_1, data for a much larger number of cycles must be acquired for accurate evaluation of the ensemble averaged velocity variation. In the uncertainty analysis the flow was modeled for 210 cycles, the number of cycles over which experimental data were ensemble averaged. A Gaussian distribution about u was assumed for u' and u'_r at a given y/δ_s was taken as that measured for oscillating flows. (The variation in turbulence level measured for oscillating flows is discussed in a later section.) Next, at each of the 20 points in the cycle, 210 u' values were generated by random entries onto the Gaussian distribution curve defined by the value of u'_r. These were superposed on the assumed ensemble averaged velocity variation, thus producing data that simulate the instantaneous velocity values determined from hot wire measurements. These data, when ensemble averaged, yield values of u_m, u_1, and ϕ, which differ from the input values because of the superposed random u' values. By repeating this simulation process at a given y/δ_s a large number of times, the uncertainties in terms of standard deviations for u_m, u_1 and ϕ could be estimated. Figure 10 presents uncertainties determined in this manner for u_1 and ϕ in terms of y/δ_s for flows produced with an oscillator wedge stroke of 1.91 cm. The uncertainty for u_m is not shown since it is an order of magnitude smaller than that for u_1. As expected, in the free stream where the turbulence level is small compared to u_1, the uncertainty is small for both u_1 and ϕ. As the wall is approached, u'_r increases and u_1 decreases, resulting in larger uncertainties in u_1 and ϕ.

Other sources of uncertainty for the results for oscillating flows include uncertainties in frequency of oscillation, δ_s, hot wire position y,

and, for u_1/U_1, the hot wire calibration. Use of a dial micrometer for positioning the hot wire resulted in very small uncertainties in y. The uncertainty in δ_s was estimated to be ± 4 percent. Thus, the uncertainty in y/δ_s was ± 4 percent. Estimates of the uncertainty of results were made by combining the uncertainties from the sources using the method of Kline and McClintock (1953). The uncertainty range ($\pm\sigma$) in Figure 8 for u_1/U_1 from all factors was estimated to be the symbol size (± 2 percent) at large y/δ_s and twice the symbol size (± 4 percent) at small values of y/δ_s. Hence, the uncertainty for u_1/U_1 is a relatively small.

The results for ϕ in Figure 9 involve larger uncertainties. An analysis of the uncertainty in ϕ due to an uncertainty of ± 0.5 percent in frequency of oscillation for the experiments yielded $\sigma_\phi = \pm 0.5$ degrees. Combining of this uncertainty with that from Figure 10 for ϕ yielded an estimate of the total σ_ϕ that ranged from ± 0.5 degrees in the free stream to ± 1 degree at $y/\delta_s = 0.05$. Bars indicating the uncertainty range on ϕ are shown on selected curves drawn through the data points in Figure 9.

Results in the form presented in Figures 8 and 9 permit assessment of the boundary layer behavior at fixed axial positions as frequency varies. Several observations can be made from these results. The results for u_1/U_1 will be considered first. It is noted in Figure 8 that the influence of unsteadiness extends beyond the steady boundary layer thickness to values of about $1.4\delta_s$ at each ξ position. Significant changes in u_1/U_1 profiles occur at a fixed position as frequency changes, as evidenced for example by the profiles at $\xi = 1.12$ m, Figure 8b. As frequency increases, u_1/U_1 is larger than unity in an increasing portion of the boundary layer and the maximum value of u_1/U_1 increases. This trend continues to a frequency of 21.3 Hz. The profile at the largest value of frequency, 29.4 Hz, exhibits

a smaller maximum value of u_1/U_1 that occurs nearer the wall. The collective results in Figure 8 can also be discussed in terms of the reduced frequency. At low reduced frequency (data set A1 in Figure 8a and data set C2 in Figure 8b, for which $\bar{\omega} = 0.54$) the profiles exhibit u_1/U_1 values that are slightly larger than unity in a small portion of the boundary layer. Beyond $\bar{\omega} = 0.54$ for flows with $\bar{\omega}$ ranging to 3, the profiles show $u_1/U_1 > 1$ for increasingly larger portions of the boundary layer. There is also a trend to larger maximum values for u_1/U_1 that occur at smaller values of y/δ_s. For flows with $\bar{\omega} > 3$ (data set C6 in Figure 8b and data set D6, Figure 8c) the fraction of the boundary layer for which $u_1/U_1 > 1$ decreases, as does the maximum value of u_1/U_1 and the value of y/δ_s at which the maximum occurs.

The profiles for the phase angle ϕ, Figure 9, show an influence of frequency of oscillation to y values of about $1.5\delta_s$ and exhibit pronounced effects of frequency. The results for $\xi = 1.12$ m in Figure 9b are somewhat typical. At the two lowest frequencies ϕ is positive throughout the boundary layer and exhibits a maximum at about $y/\delta_s = 0.3$. As frequency increases, regions of negative ϕ develop toward the outer part of the boundary layer. Quite large negative values occur at the higher frequencies near $y/\delta_s = 0.8$ As y/δ_s decreases, ϕ becomes positive, and at a frequency of 21.3 Hz, the curve clearly exhibits a maximum value at a low value of y/δ_s. Due to the uncertainty in ϕ of ± 1 degree at low y/δ_s and the sparseness of the data near the wall, the tendency to exhibits maximum is less clear for the results at a frequency of 29.4 Hz (data set C6). The results at $\xi = 1.58$ m, Figure 9c, exhibit characteristics similar to those at $\xi = 1.12$ m, while at $\xi = 0.61$ m (Figure 9a), the profiles generally show only increasing values of ϕ as the wall is approached.

The results in Figures 8 and 9 were obtained for flows generated with a wedge stroke of 1.91 cm. Table 2 lists four data sets that were obtained with shorter wedge strokes, and therefore had smaller amplitudes of oscillation. Except for amplitude of oscillation, the parameters for these four data sets, A5, C5, D5, and D7, respectively match or closely match data sets A4, C4, D4, and D6. Comparisons of the matched data sets are presented in Figures 11 and 12. The profiles of u_1/U_1 for data sets A4 and A5 for which $\xi = 0.61$ m and the frequency is 21 Hz are shown in Figure 11a. Although the local value of U_1/U_m for data set A5 is two-thirds of that for data set A4, there is only a small difference in the profiles and this occurs at low values of y/δ_s. U_1/U_m for data set C5 is about two-thirds of that for data set C4. The comparison in Figure 11b for data sets C4 and C5 show no detectable influence of amplitude of oscillation. The profiles for data sets D4 and D5, Figure 11c, are also essentially identical. The local value of U_1/U_m for data set D5 is 60 percent of U_1/U_m for data set D4. Figure 11c also shows profiles for data sets D6 and D7. These profiles, for which the frequency is 21 Hz, exhibit a difference for the full range of y/δ_s. The local value of U_1/U_m for data set D7 is one-half of that for data set D6.

Comparisons showing the influence of amplitude of oscillation on ϕ profiles are presented in Figure 12. The profiles for data sets A4 and A5 show a small but distinct difference near $y/\delta_s = 1$. Near the wall, the difference is about the size of the uncertainty in the angle measurements. (Due to the smaller amplitude of oscillation relative the the turbulence level in the boundary layer, uncertainties in results obtained at the shorter wedge strokes are larger than those for the 1.91 cm stroke.) The same situation exists in the comparisons of data sets C4 and C5, Figure

12b, and D4 and D5, Figure 12c. Within the uncertainty of the results, the profiles for data sets D6 and D7 show little difference over the full range of y/δ_s. Inspection of Figures 12 and 13 leads to the conclusion that for the flows investigated, the amplitude of velocity oscillation has at most a small influence on the boundary layer behavior.

Figures 13 and 14 present profiles of u_1/U_1 and ϕ in terms of y/δ_s for three values of frequency; 7 Hz, 15 Hz, and 21 Hz. All data sets at or near these frequencies are included in the figures. For data sets where conditions were the same except for wedge stroke and for which results were nearly the same, a single curve has been drawn through the collective data points for clarity. The results in Figures 13 and 14 allow visualization of the evolution of profiles for u_1 and ϕ as functions of axial location at fixed values of frequency. In interpreting these results it is necessary to take into account the phase shift in the free stream velocity that occurs in the direction of flow at a fixed frequency as described in Figure 6.

As previously mentioned, experiments were performed at discrete values of reduced frequency to assess the extent to which $\bar{\omega}$ serves as a correlating variable for results of the boundary layer velocity surveys. As indicated in Table 2, data were obtained at different ξ locations for reduced frequencies at or near 1.0, 2.2, 3.0, and 4.1. Figures 15 and 16 show u_1/U_1 and ϕ profiles for boundary layers generated at these values of $\bar{\omega}$. While there are some differences in both the u_1/U_1 and ϕ profiles within the results at each of the four values of $\bar{\omega}$, it is clear that the profiles group more closely than do the profiles at fixed values of position alone, Figures 8 and 9, or frequency alone, Figures 13 and 14. Thus, within the range of flows investigated, the results tend to group

fairly closely when plotted in terms of the y/δ_s and at fixed $\bar{\omega}$.

5.3 Turbulence Level in Oscillating flows

The measurements made in oscillating flows that yielded the boundary layer velocity variation also provided data for assessment of the level of longitudinal turbulence. These data form the basis for investigating possible time-dependent effects on turbulence in the oscillating flows studied. Time-dependent effects can be detected by comparing measured levels of turbulence in the boundary layer with those for quasi-steady flows, i.e., flows for which no time-dependent effects are present. In a quasi-steady (slowly varying) oscillating boundary layer flow, the turbulence level at a fixed value of ξ and a given y value, as indicated by u'_r at the point, would vary periodically due to change in the boundary layer thickness that results from variation in the free stream velocity. This variation can be predicted for a given free stream velocity by use of the measured steady flow profiles for u/U_m and u'_r/u in Figures 4a and 4c. From the relation

$$\delta/x = 0.37/(U\xi/\nu)^{0.2}$$

for an incompressible zero pressure gradient turbulent boundary layer with a 1/7 power velocity profile, δ is proportional to $U^{-0.2}$. Thus, the variation in δ is 180 degrees out of phase with the free stream velocity variation, i.e., an increasing free stream velocity U produces a decreasing δ. From Figure 4c, it is seen that since y is fixed, this results in a variation in u'_r/u that is also 180 degrees out of phase with the velocity variation. The variation in u, the local boundary layer velocity, is in phase with the free stream velocity, as is the variation in u/U. The latter can be deduced from Figure 4a and the fact that the variation in δ is out of phase with the free stream velocity. In computing $u'_r = (u'_r/u)u$

for the varying free stream velocity, u dominates, with the result that the variation in u'_r is in phase with the free stream velocity. Thus, a sinusoidal variation in the free stream velocity in the form $U = U_m + U_1 \text{Cos}\ \omega t$ produces a quasi-steady boundary layer velocity variation of the form $u(y,t) = u_m(y) + u_1(y) \text{Cos}\ \omega t$ and an essentially sinusoidal variation in u'_r of the form

$$u'_r(y,t) = u'_{rm}(y) + u'_{r1} \text{Cos}\ \omega t \qquad (5.1)$$

Figure 17 shows the curve of u'_{rm} vs y/δ_s computed for steady flow conditions at $\xi = 1.58$ m using the profiles for u/U_s and u'_r/u from Figures 4a and 4c. Thus the curve represents the measured variation in u'_{rm} with y/δ_s and is applicable to both steady and quasi-steady flows. The amplitude u'_{r1} depends directly on the amplitude of the free stream velocity U_1, which in turn depends on the wedge stroke. Experimental results for u'_r obtained at three frequencies of oscillation and two wedge strokes at $\xi = 1.58$ m (results from data sets D1, D4, D5, D6, and D7) are presented in Figure 17 and will be discussed subsequently. The broken lines in Figure 17 above and below the u'_{rm} curves show the extremes of equation (5.1) determined for free stream conditions corresponding to each of the five data sets noted. Data sets D1, D4, and D6 were obtained with a wedge stroke of 1.91 cm, while data sets D5 and D7 were obtained at shorter strokes. The quasi-steady amplitude u'_{r1} for data set D5 is smaller than u'_{r1} for data set D4 by approximately the ratio of the amplitudes of the free stream velocities, which is given by the ratio of the values for U_1/U_m for the two data sets. From Table 2 the value of this ratio is 0.071/0.121 = 0.59. Similarly, the quasi-steady value for u'_{r1} for data set D7 is one half that for data set D6 because U_1 for D7 was one-half that for D6. It is useful to compare the amplitude of oscillation of u'_r to that of the

local velocity variation for quasi-steady oscillating flow. Due to the fact that U_1/U_m for the oscillating flows investigated at $\xi = 1.58$ m was relatively small (0.136 or smaller), the ratio u'_{r1}/u_1 for quasi-steady flows at a fixed y value is essentially independent of wedge stroke. Figure 18 shows the curve computed for u'_{r1}/u_1 for quasi-steady flow at $\xi =$ 1.58 m.

As noted above, an essentially sinusoidal variation was predicted for u'_r in quasi-steady flows. A sinusoidal variation for u'_r is also indicated by the measurements of u'_r. This is illustrated in Figure 19 in which experimental results for u'_r and the corresponding fitted cosine curves are shown at two values of y/δ_s for oscillating flows from data set D6. Although the results were determined from ensemble-averaging hot wire measurements for 210 cycles, there is scatter in the data points about the fitted curves. This scatter is directly related to the turbulence level in the flow. However, the variations are clearly sinusoidal in nature. It is also evident that the variations for u'_r shown are not in phase. Fitted curves like those in Figure 19 provide a means of displaying the behavior of u'_r measured in the boundary layer. It is useful to make comparisons with the local boundary layer velocity

$$u(y,t) = u_m(y) + u_1(y)\mathrm{Cos}[\omega t + \phi(y)] \qquad (1.2)$$

by writing for the experimental variation in u'_r

$$u'_r(y,t) = u'_{rm} + u'_{r1}\mathrm{Cos}[\omega t + \phi(y) - \beta(y)] \qquad (5.2)$$

Thus, $\beta(y)$ is the phase angle by which u'_r lags u. (In quasi-steady oscillating flows both ϕ and β are zero.) In Figure 17, the symbols denote measured values of u'_{rm} and the vertical solid lines indicate the extremes of the fitted cosine curves, such as those in Figure 19, as given by equation (5.2). For each of the oscillating flows considered, the

experimental results for u'_{rm} differ somewhat from u'_{rm} for quasi-steady flow (that measured for steady flow). Except for data set D5, the results indicate measured u'_{rm} values that are slightly above the quasi-steady curve for u'_{rm}. Also, for most of the range of y/δ_s, the amplitudes of oscillation, u'_{r1}, tend for each data set to differ from those for quasi steady oscillating flow. This is particularly evident near $y/\delta_s = 1$. This is also observed in Figure 18 which shows values for the ratio u'_{r1}/u_1 determined from the measurements for each of the oscillating flows considered in Figure 17. The results in Figure 18 are grouped in terms of frequency. Although there is scatter in the results at each frequency, the data exhibit variations that clearly differ from the quasi-steady distribution of u'_{r1}/u_1 vs y/δ_s. At 5.04 Hz, the difference is most evident near $y/\delta_s = 1$. The difference between quasi-steady and experimental results at the two other frequencies are even more pronounced, with the largest values for u'_{r1}/u_1 occurring at small values of y/δ_s and at values of y/δ_s near unity. The experimental results for 15.5 and 21 Hz show essentially the same trend, and within the scatter of the results, no effect of amplitude of velocity oscillation on the results is evident, as indicated by the essential agreement between results for data sets D4 and D5 at 15.5 Hz and data sets D6 and D7 at 21 Hz. This indicates that at a given point in an oscillating flow u'_{r1} depends directly on u_1. However, the ratio u'_{r1}/u_1 is frequency dependent.

The variation in the phase angle β with y/δ_s gives further evidence of time-dependent effects on turbulence in the oscillating flows investigated. The measured variations of β are shown in Figure 20 for data sets D1, D4, D5, D6, and D7 and are grouped in terms of frequency. The results indicate that u'_r lags the local boundary layer velocity u by an increasingly larger

angle as y/δ_s increases and that large changes in β occur across the boundary layer. Different variations of β with y/δ_s are indicated for each of the three values of frequency. However, there is no evident effect of amplitude of velocity oscillation on β, as indicated by the reasonable agreement of results for data sets D4 and D5 as well as for data sets D6 and D7. It is evident from the collective results in Figures 17 to 20 that there are significant effects of unsteadiness on turbulence in the oscillating flows investigated at $\xi = 1.58$ m. The time-dependent turbulence can be described with reasonable accuracy by use of equation (5.2) and the results in the figures. Turbulence levels measured at $\xi =$ 0.61 and 1.12 m exhibit time-dependent effects that differ somewhat from those at $\xi = 1.58$ m but are similar in nature.

6. NUMERICAL METHOD FOR PREDICTING BOUNDARY LAYER BEHAVIOR

The governing equations for the flows under consideration were taken as the ensemble averaged incompressible unsteady boundary layer equations incorporating a scalar eddy viscosity relation between stress and strain. These equations are

$$\frac{\partial u}{\partial x} + \frac{\partial v}{\partial x} = 0 \tag{6.1}$$

$$\frac{\partial u}{\partial t} + u\,\frac{\partial u}{\partial x} + v\,\frac{\partial u}{\partial y} = -\frac{1}{\rho}\,\frac{\partial p}{\partial x} + \nu\,\frac{\partial}{\partial y}\left(1 + \frac{\varepsilon}{\nu}\right)\frac{\partial u}{\partial y} \tag{6.2}$$

Following McCroskey and Phillipe (1975) the following coordinate transformation is introduced: $(x,y,t)\rightarrow(\xi,\eta,t)$ where ξ is the distance from the turbulent boundary layer origin (the trip wire in Figure 1.), $\eta = (U/2\xi\nu)^{1/2}$, and $\tau = \omega t$. This yields

$$\left.\begin{aligned} &\xi\,\frac{\partial \bar{u}}{\partial \xi} + \frac{\partial V}{\partial \eta} - \frac{\beta_t}{2} + \frac{\bar{u}}{2}\,(\beta_x + 1) = 0 \\ &\frac{\xi\omega}{U}\,\frac{\partial \bar{u}}{\partial \tau} + \xi\bar{u}\,\frac{\partial \bar{u}}{\partial \xi} + V\,\frac{\partial \bar{u}}{\partial \eta} + (\bar{u} - 1)\beta_t \\ &\qquad + (\bar{u}^2 - 1)\beta_x - \frac{1}{2}\,\frac{\partial}{\partial \eta}\,(1 + \bar{\varepsilon})\,\frac{\partial \bar{u}}{\partial \eta} = 0 \end{aligned}\right\} \tag{6.3}$$

where

$$\beta_t = \frac{\omega\xi}{U^2}\frac{\partial U}{\partial \tau}, \qquad \beta_x = \frac{\xi}{U}\frac{\partial U}{\partial \xi},$$

$$V = \frac{\eta}{2}\beta_t + \bar{u}\frac{\eta}{2}(\beta_x - 1) + \bar{v}\left(\frac{U\xi}{2\nu}\right)^{\frac{1}{2}}, \quad \bar{u} = \frac{u}{U}, \ \bar{v} = \frac{v}{U} \tag{6.4}$$

and ε is the dimensionless eddy viscosity. The latter parameter is taken in the present study from either the well-known Cebeci-Smith algebraic model (1968) or the one-equation model of Glushko (1965). The Glushko model uses a single differential equation to describe the transport of turbulence kinetic energy in conjunction with an algebraic scale equation and includes a time-dependence in the turbulence field as well as the velocity field. It is the simplest available model that explicitly admits time-dependence in the turbulence field as distinguished from the mean velocity field.

The pressure gradient in equation (6.2) is related to the free stream velocity U by

$$-\frac{1}{\rho}\frac{\partial p}{\partial x} = \frac{\partial U}{\partial t} + U\frac{\partial U}{\partial x} \tag{6.5}$$

and to β_t and β_x in equation (6.4) by

$$-\frac{1}{\rho}\frac{\partial p}{\partial \xi} = \frac{U^2}{\xi}(\beta_t + \beta_x) \tag{6.6}$$

Thus it is evident that the solution of the governing equations depends on the manner in U varies with position and time in the test section. This variation in turn depends on how the flow is generated and may differ between experimental facilities. As previously noted, $U = U(x,t)$ can be predicted analytically for the present facility as $a_m M(x,t)$, where $M(x,t)$ is given by equation (2.2). Thus the terms β_t and β_x in equations (6.3) as given in equation (6.4) can be determined.

It is useful to examine the nature of the pressure gradient generated in the present flows since the pressure gradient, particularly its phase

relative to the free stream velocity, has a significant effect on the boundary layer behavior. In this analysis, pressure gradients generated in flows with small amplitudes of velocity will be considered. It is convenient to write the pressure gradient term, equation (6.5), in dimensionless form as

$$-\frac{\partial P}{\partial x} = \frac{\omega}{a_m}\frac{\partial M}{\partial \omega t} + M_m\frac{\partial M}{\partial x} \tag{6.7}$$

where $P = p/(kp_m)$. Substitution of $M(x,t)$ from equation (2.2) into equation (6.7) yields

$$-\frac{\partial P}{\partial x} = G(x)\ \mathrm{Cos}[\omega t + \Delta(x) - \Gamma(x)] \tag{6.8}$$

where

$$G(x) = \left([-M_m S'(x)]^2 + [\frac{\omega}{a_m}\ S(x) + M_m S(x)\Delta'(x)]^2\right)^{1/2} \tag{6.9}$$

and

$$\Gamma(x) = \tan^{-1}\frac{S(x)[\frac{\omega}{a_m} + M_m\Delta'(x)]}{-M_m S'(x)} \tag{6.10}$$

The angle Ψ by which the pressure gradient leads the free stream Mach number (velocity) variation can be determined by comparing the cosine functions in equations (2.2) and (6.8). At a fixed x, $\cos(\omega t + \Delta)$ leads $-\mathrm{Cos}(\omega t + \Delta)$ by π radians. Also, $\mathrm{Cos}(\omega t + \Delta - \Gamma)$ lags $\cos(\omega t + \Delta)$ by Γ radians. Thus, $\mathrm{Cos}(\omega t + \Delta - \Gamma)$ leads $-\cos(\omega t + \Delta)$ by

$$\Psi(x) = \pi - \Gamma(x) \tag{6.11}$$

Figure 21 shows $G(x)$ and $\Gamma(x)$ in equation (6.8) at three values of frequency. At low frequency the terms $S'(x)$, $\Delta(x)$, and $\Delta'(x)$ in equations (6.9) and (6.10) are small, as can be seen from examination of Figure 6. Thus the variation of G and Γ with x is small, Γ is close to $\pi/2$, and Ψ is essentially $\pi/2$. Hence, the pressure gradient $-\partial P/\partial x$ leads the free stream velocity by $\pi/2$. With increasing frequency, G and Γ depend increasingly on

x, which results in Ψ increasing to values larger than but near $\pi/2$.

The influence of the phase relation between the pressure gradient and the free stream velocity on boundary layer behavior can be addressed by considering an analysis developed by Patel (1977). Patel considered a free stream velocity variation of the form

$$U(x,t) = U_m + U_1 e^{i\omega[t - (x/Q)]} \qquad (6.12)$$

in which $Q = KU_m$ is called the travelling wave convection velocity and U_m, U_1, and K are constants. The pressure gradient produced by U(x,t) in equation (6.12) is

$$-\frac{1}{\rho}\frac{\partial p}{\partial x} = i\,\omega\left[U_1\, e^{i\,\omega(t - x/Q)}\right] - i\,\omega\frac{U_m}{Q}\left[U_1\, e^{i\,\omega(t - x/Q)}\right] \qquad (6.13)$$

For $Q = \infty$, equation (6.13) shows that the pressure gradient leads the velocity by $\pi/2$ radians. Facilities of the type used by Karlsson (1973) and Coustiex, et al (1973), (and, as noted, the present facility) produce flows in which the pressure gradient leads the free stream velocity by approximately $\pi/2$ radians. However, Patel's facility generated flows with $Q = 0.77\ U_m$, which results in a pressure gradient that lags the velocity by $\pi/2$ radians. As a result, an oscillating-flow boundary layer behavior significantly different from that observed in this study or reported in the studies of Karlsson and Cousteix was recorded by Patel. For example, Patel observed the maximum value for the boundary layer velocity amplitude ratio u_1/U_1 at $\bar{\omega} = 4$ to be 1.55, while in the present study this value is seen to be about 1.1 in Figure 15d. In addition, Patel recorded large negative phase angles in most of the boundary layer, while in the present study phase angles are generally both positive negative (see Figure 16). This difference is explained as follows. For $Q/U_m = 1$, equation (6.13)

indicates that the pressure gradient is zero. For this case only viscous forces act in the boundary layer. Patel's analysis shows that this produces a boundary layer velocity variation that generally lags the free stream velocity and has relatively small amplitude of oscillation. When, as in Patel's experimental study, a lagging pressure gradient also acts on the flow, the viscous and pressure gradient forces act somewhat in phase to produce large amplitudes of oscillation in the boundary layer as well as large phase lags relative to the free stream flow. However, a leading pressure gradient acts out of phase with the viscous forces and produces smaller amplitudes of oscillation and positive values of the phase angle ϕ except possibly near the boundary layer edge, as observed in the present study.

The numerical method employed to solve equations (6.3) was developed by Murphy and Prenter (1981). It uses splined cubic Hermite polynomials to represent the stream-normal variation of the flow parameters, with the coefficients of these polynomials determined by orthogonal collocation. The stream wise derivatives are represented by classical second-order accurate finite difference approximations and the temporal variation cum linearization is accomplished by either a Crank-Nicolson method or by second order accurate finite difference with Newton-Raphson iteration. The choice of iterative or noniterative time marching is made by the user. The result is a hybrid finite-element finite-difference scheme which if fourth order accurate in y and second-order accurate in x and t. The high accuracy in the stream normal direction is consistent with the boundary layer assumptions and permits accurate solutions on a relatively coarse mesh.

7. COMPARISONS OF EXPERIMENTAL AND PREDICTED BOUNDARY LAYER BEHAVIOR

Computations using both the Cebeci-Smith and Glushko turbulence models were performed to predict the behavior for several the oscillating turbulent boundary layer cases studied experimentally at $\xi = 1.58$ m. Figure 22a shows the mean velocity profiles predicted by numerical computations using both turbulence models. The numerical method with either turbulence model predicts slightly higher velocity values in the boundary layer than were experimentally observed. Figures 22b and 22c compare predicted and experimental results for u_1/U_1 and the phase angle ϕ at four frequencies. Predicted results are shown for both turbulence models. While the predicted and experimental results are not in exact agreement for either turbulence model, the results obtained using the Glushko model are generally inferior to those obtained from the Cebeci Smith model. Therefore the discussion will focus on the results predicted using the Cebeci-Smith model. In all cases these results do not show a significant influence of unsteadiness beyond $y/\delta_s = 1$, while the experimental results do. At frequencies 5.04 Hz and 11.3 Hz the experimental and predicted results for both u_1/U_1 and ϕ are in fair agreement. At frequencies 15.5 Hz and 21.0 Hz larger differences between the predicted and experimental results exist, with the exception of u_1/U_1 at $f = 21$ Hz. With the exception of the results at 21 Hz, the predicted curves for ϕ exhibit increasing values with decreasing y/δ_s for the full range of y/δ_s, while the experimental corresponding results (at least the results a 5.04 Hz) exhibit a maximum value of ϕ at $y/\delta_s > 0$ and then show decreasing values of ϕ as y/δ_s decreases. The predicted results for ϕ at 21 Hz exhibit characteristics similar to other predicted results for ϕ, except negative angles are predicted near $y/\delta_s = 0.8$. For all frequencies

significant differences exist between the Cebeci-Smith predicted results and the experimental results for y/δ_s less than about 0.1. The behavior of the phase angle near the wall is similar to that found by Cousteix (1981). Thus there appears to be no reason to question the present results. Near the wall the results obtained using the Glushko turbulence model differ only in magnitude from those obtained using the Cebeci-Smith model. It is likely that the disagreement between predicted and experimental results both near the wall and in the remainder of the boundary layer is due at least in part to failure of the turbulence models to adequately describe viscous effects in the unsteady flows involved.

8. SUMMARY

The oscillating flows studied experimentally cover a wide range of frequency and reduced frequency. This study was made possible because the facility used to generate the time-dependent flows produces an essentially pure sinusoidal variation in free stream velocity at all frequencies. The study has yielded a quantitative description of the boundary velocity variation for y/δ_s greater than about 0.05 at fixed axial positions as a function of frequency, fixed frequencies as a function of position, and at fixed values of reduced frequency $\bar{\omega}$. Mean velocity profiles, u_m/U_m vs y/δ_s, were found to exhibit only small deviations from corresponding steady flow profiles. The boundary layer velocity amplitude ratio u_1/U_1 and phase angle ϕ relative to the free stream flow were generally found to depend strongly on position and frequency. When plotted in terms of y/δ_s at fixed $\bar{\omega}$ profiles for u_1/U_1 and ϕ tended to collapse toward single curves, indicating usefulness of $\bar{\omega}$ as a similarity parameter for correlating results for the oscillating flows examined.

The longitudinal turbulence level, as indicated by the measured

variation in u'_r for the ensemble averaged cycle, was found to be strongly time-dependent. Quantitative results for turbulence level are presented for flows at $\xi = 1.58$ m. The mean value of u'_r was found to be close to that measured for steady flow for all frequencies. However, the amplitude of u'_r and the phase relation between u'_r and the local boundary layer velocity u exhibited significant differences from those predicted for quasi-steady flows. The amplitude of u'_r was found to vary with y/δ_s. In addition, at frequencies above about 15 Hz large amplitudes of oscillation in u'_r occurred both near the wall and near $y/\delta_s = 1$. The phase relation between u'_r and u varied in a pronounced manner across the boundary layer.

The experimental study of the effects of amplitude of free stream velocity on boundary layer behavior was conducted for a limited range of U_1/U_m. Boundary layer velocity profiles quantities, u_1/U_1 and ϕ, exhibited at most a small influence of amplitude of oscillation. Similarly, u'_r/u_1 as well as the phase angle between u'_r and the local velocity in the boundary layer showed no influence of amplitude of free stream velocity.

The numerical method described for predicting boundary layer behavior in the time dependent flows studied was applied using the turbulence models of Cebeci and Smith, and of Glushko. The required boundary condition at the boundary layer edge, the free stream velocity, was supplied using analytical expressions developed for the present facility. These expressions predict variations in amplitude with position and frequency and corresponding phase relations for the free stream flow. Somewhat different velocity variations in the boundary layer are predicted by the numerical method when the two turbulence models are used. Generally the Cebeci-Smith model produces results that are in best agreement with the experiments. Numerical results obtained using the Cebeci-Smith model are in many

respects qualitatively correct. The differences that exist between the numerical predictions and measured results are apparently due at least in part to the inadequacy of the turbulence models.

REFERENCES

Brembati, F. 1975 Project Report, Von Karman Inst. of Fluid Dynamics, Rhode Saint Genese, Belgium

Brederode, V. de & Bradshaw, P. 1978 J. Fluids Engng 100, 91-95.

Carr, L. W. 1981 NASA TM 81279

Cebeci, T. & Smith, A. M. O. 1968 Proc. AFOSR-IFP-Stanford Conference on Computation of Turbulent Boundary Layers

Coles, D. E. 1968 Proc. AFOSR-IFP-Stanford Conference on Computation of Turbulent Boundary Layers 2, 1-45.

Cousteix, J., Desopper, A. & Houdeville, R. 1977 Proc. Symp on Turbulent Shear Flows, Pa. State Univ., 18-20, April. Also Turbulent Shear Flows I, (F. Durst, Ed.) Springer Verlag, 1979.

Cousteix, J., Houdiville, R. & Javelle, J. 1981 Turbulent Shear Flows 3, Springer Verlag, (L. J. S. Bradbury, et al, eds), 46-59.

Glushko, G. S. 1965 NASA TT F-10080.

Karlsson, S. K. F. 1959 J. Fluid Mech. 5, 622-636.

Kline, S, J. & McClintock, F. A. 1953 Mech. Engng 75, 3-8.

McCroskey, W. J. & Phillipe, J. J. 1975 A.I.A.A. J., 13, 71-79.

Murphy, J. D. & Prenter, P. M. 1981 Third Symp on Turbulent Shear Flows, Univ. of CA, Davis.

Patel, M. H. 1977 Proc. Royal Soc. of London A 353, 121-144.

Rao, K. N., Narasimha, R. & Badri Narayanan, M. A. 1971 J. Fluid Mech. 48, 339-352.

Simpson, R. L., Chew, Y.-T & Shivaprasad, B. G. 1981 J. Fluid Mech. 113, 23-51.

Smith, A. & Clutter, D. 1959 J. Aero. Sci. 26, 229-245.

Telionis, D. P. 1981 Unsteady Viscous Flows, Springer Verlag.

Table 1. Description of oscillating flow facility.

Entrance section
Flow-straightening section:
Diameter: 0.3 m, Length: 0.5 m
Honeycomb: 0.5 cm hex cell, 3 cm length
Screen: 0.3 solidity ratio
Contraction section:
Length: 0.3 m, Area ratio: 12 to 1
Test section
Length: 2.08 m, Cross section: 7.5 cm x 7.5 cm
Walls: 2.5 cm-thick aluminum
Boundary layer trips: 0.05 mm dia. wire on four walls at x = 0.13 m
Unit Reynolds number: 1.52×10^6/m
Wave generator
Nozzle throat cross section: 2.13 cm x 7.5 cm
Wedge: 14 degree included angle
Wedge strokes: 0.953, 1.27, 1.91 cm
Frequency: 0 to 35 Hz

Table 2. Compilation of oscillating flow boundary layer surveys

Data Set	ξ, m	f, Hz	$\bar{\omega}$	Wedge stroke, cm	U_1/U_m
A1	0.61	6.79	0.54	1.91	0.131
A2	0.61	13.1	1.05	1.91	0.142
A3	0.61	15.5	1.24	1.91	0.147
A4	0.61	20.9	1.67	1.91	0.169
A5	0.61	20.9	1.67	1.27	0.112
B1	0.91	19.1	2.24	1.91	0.132
C1	1.12	3.85	0.54	1.91	0.131
C2	1.12	7.10	1.00	1.91	0.126
C3	1.12	15.5	2.19	1.91	0.138
C4	1.12	21.3	3.01	1.91	0.152
C5	1.12	21.3	3.01	1.27	0.097
C6	1.12	29.4	4.16	1.91	0.239
D1	1.58	5.04	0.97	1.91	0.126
D2	1.58	6.79	1.31	1.91	0.126
D3	1.58	11.3	2.18	1.91	0.118
D4	1.58	15.5	2.99	1.91	0.121
D5	1.58	15.1	2.91	1.27	0.071
D6	1.58	21.0	4.05	1.91	0.136
D7	1.58	21.0	4.05	0.953	0.065

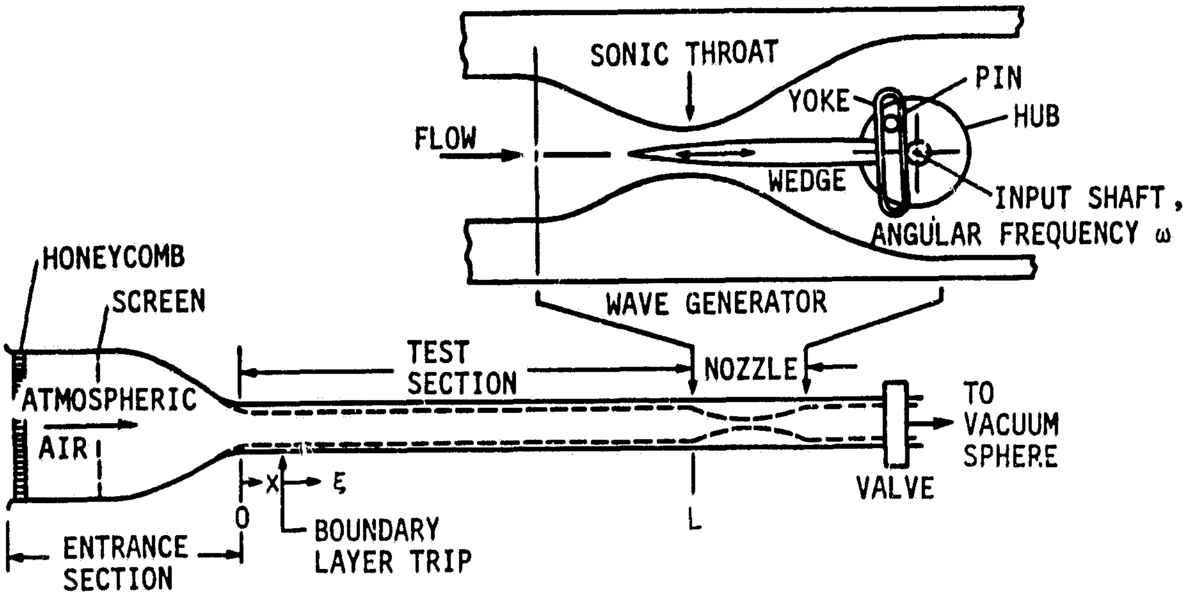

Figure 1. Oscillating flow facility.

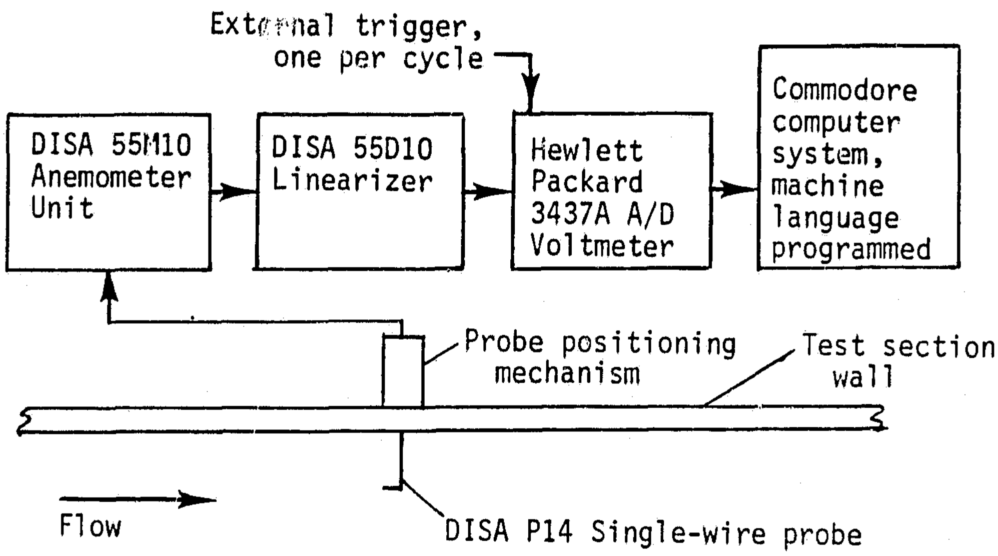

Figure 2. Data acquisition system.

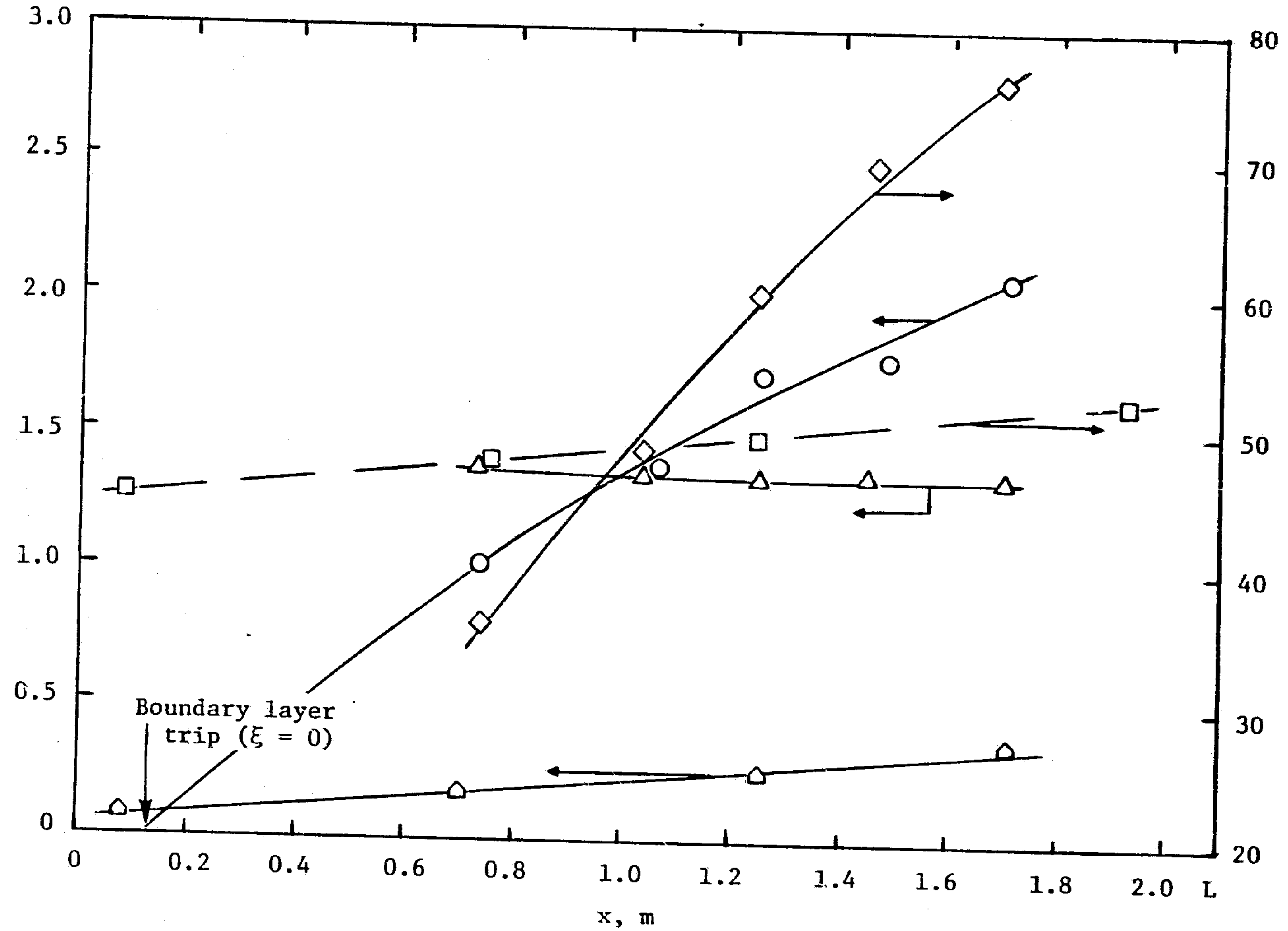

Figure 3. Measured steady flow quantities vs axial position: —◇— , $Re_\theta/100$; —○— , δ_s, $\delta_s = 1.47\xi^{0.74}$ cm; —□— , center line velocity, $U_s = 45.2 + 3.65x$ m/s; —△— , $H = \delta^*/\theta$; —⌂— , center line turbulence intensity, $100u'_r/U_s$

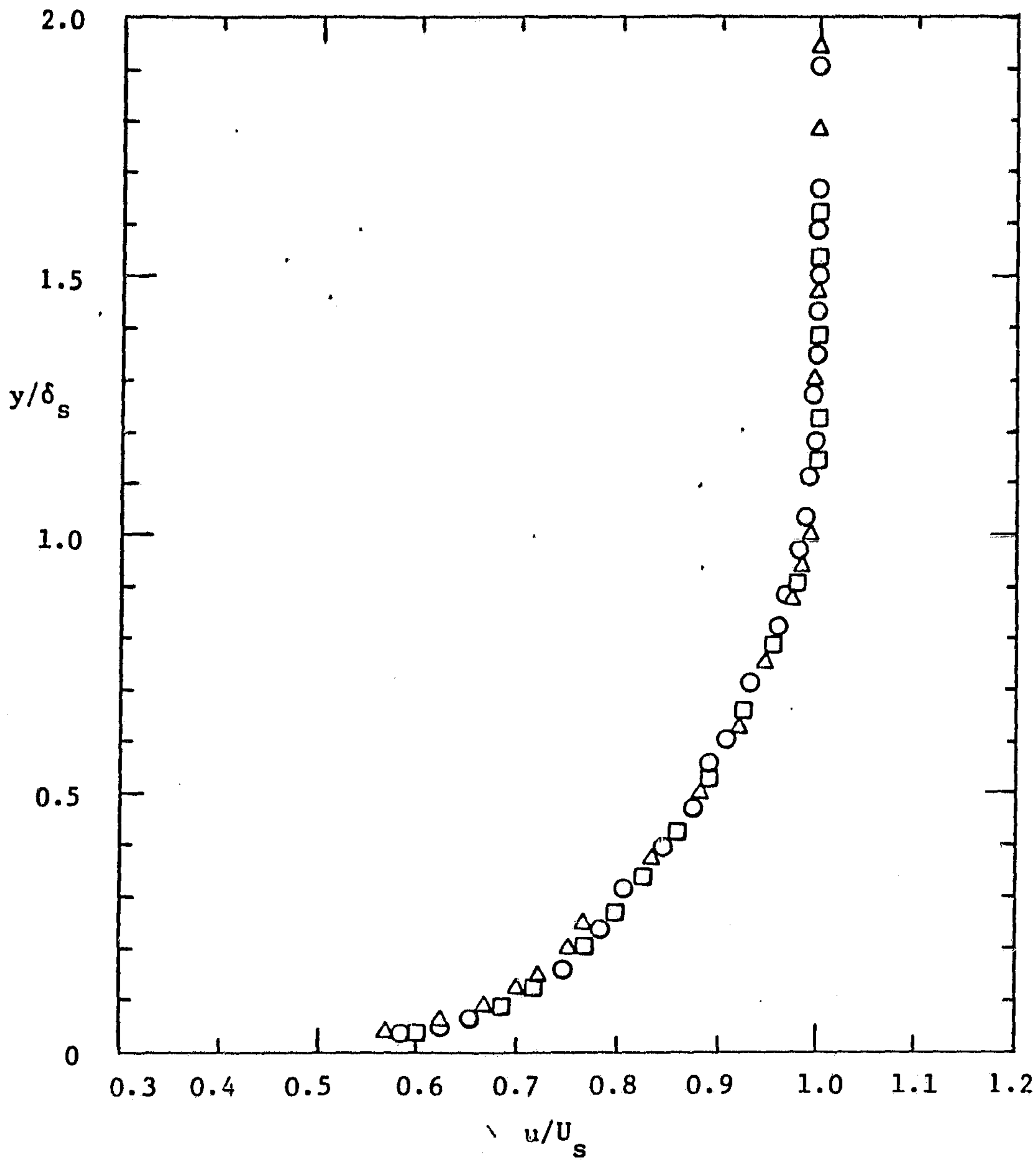

a.

Figure 4. Boundary layer velocity and turbulence intensity profiles for steady flows: Δ, ξ = 0.61 m; $\bigcirc$, ξ = 1.12 m; $\square$, ξ = 1.58 m

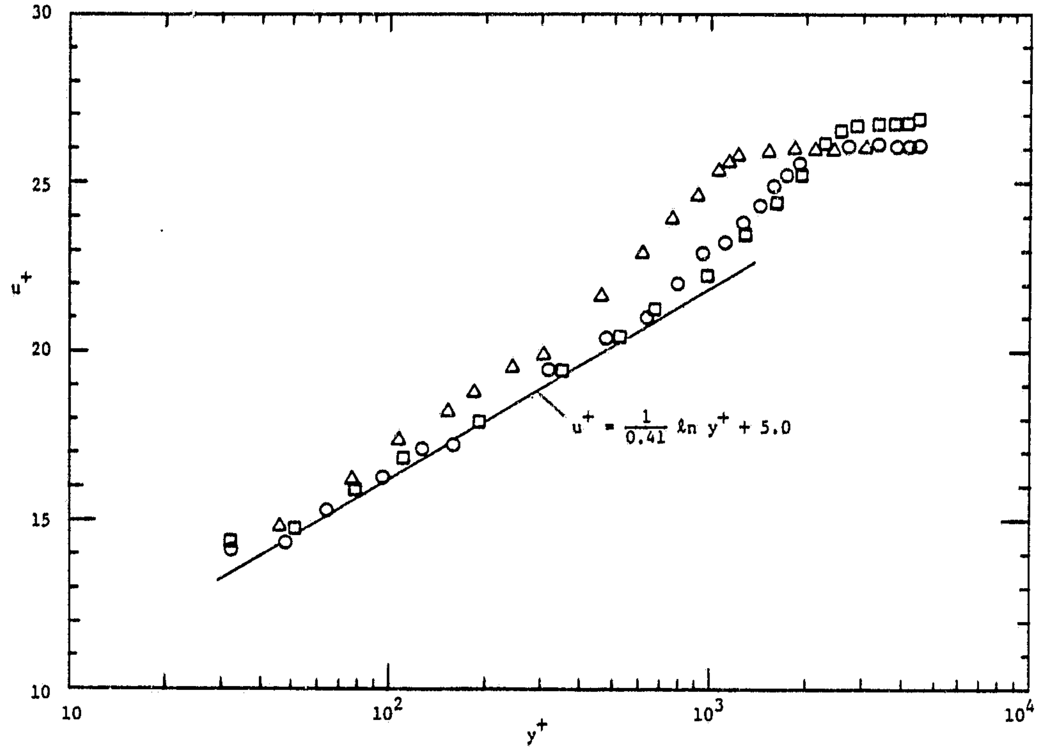

b.

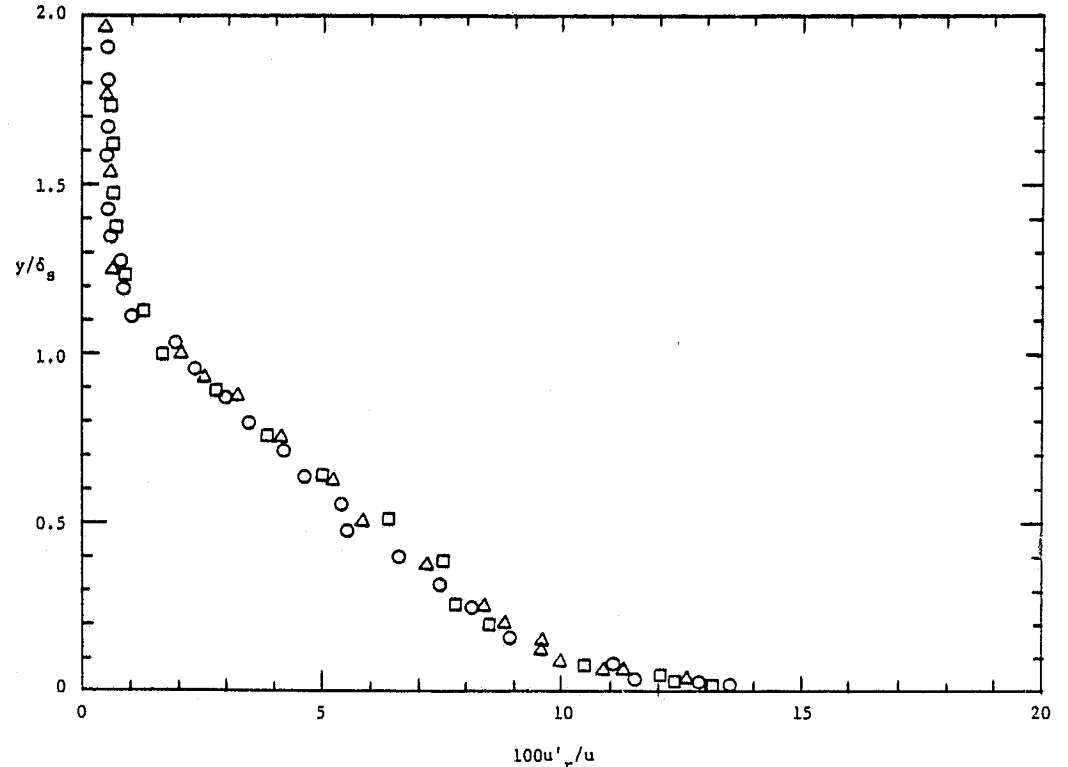

c.

Figure 4. Concluded.

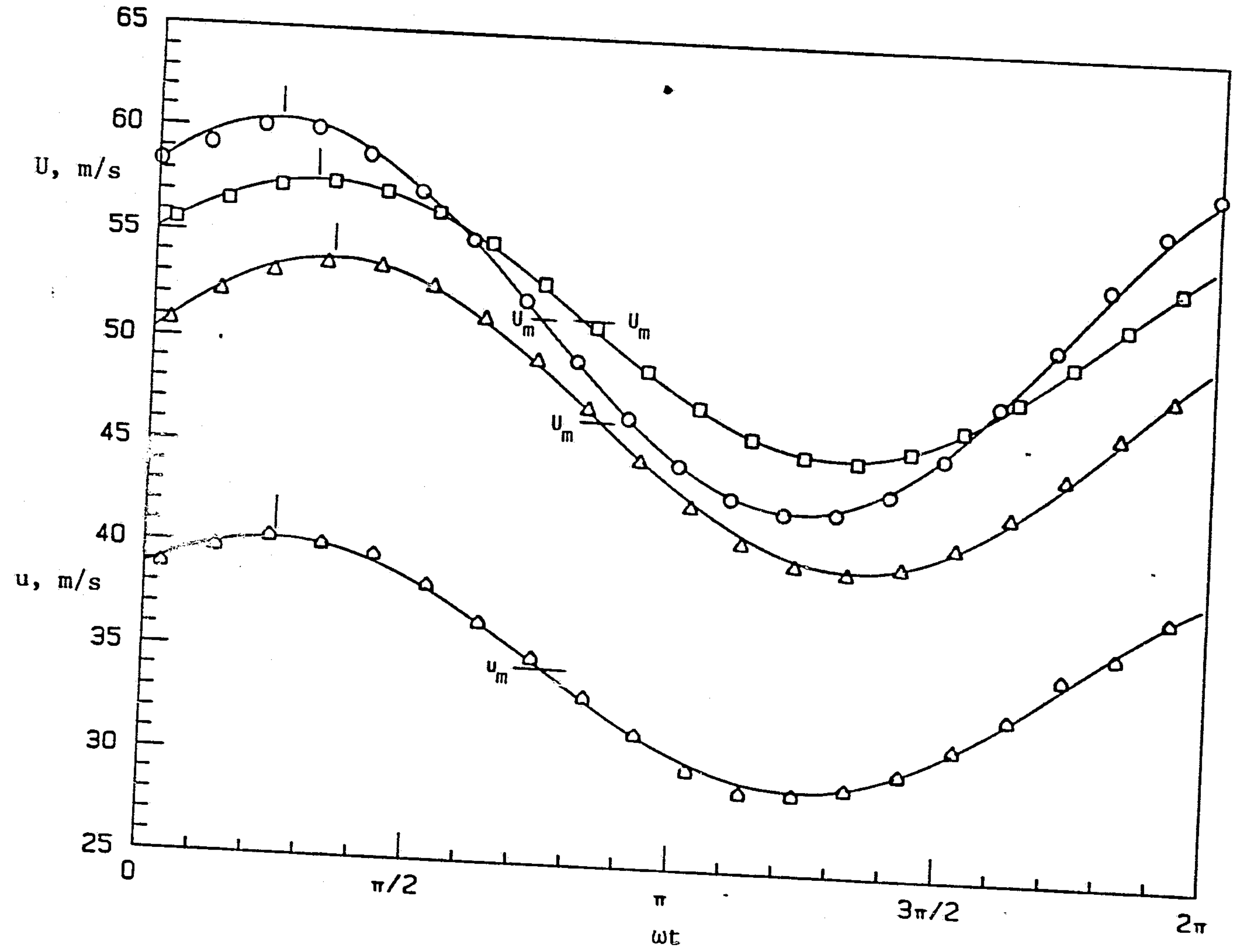

Figure 5. Experimental ensemble-averaged velocity variations. Vertical marks on curves indicate maximum values.

—○— , $\xi = 1.58$ m, $f = 29.4$ Hz, $y/\delta_s = 1.83$, $U_1 = 8.99$ m/s

—□— , $\xi = 1.58$ m, $f = 15.5$ Hz, $y/\delta_s = 1.83$, $U_1 = 6.25$ m/s

—△— , $\xi = 0.305$ m, $f = 15.5$ Hz, $y/\delta_s = 2.20$, $U_1 = 7.08$ m/s

—△— , $\xi = 1.58$ m, $f = 15.5$ Hz, $y/\delta_s = 0.10$

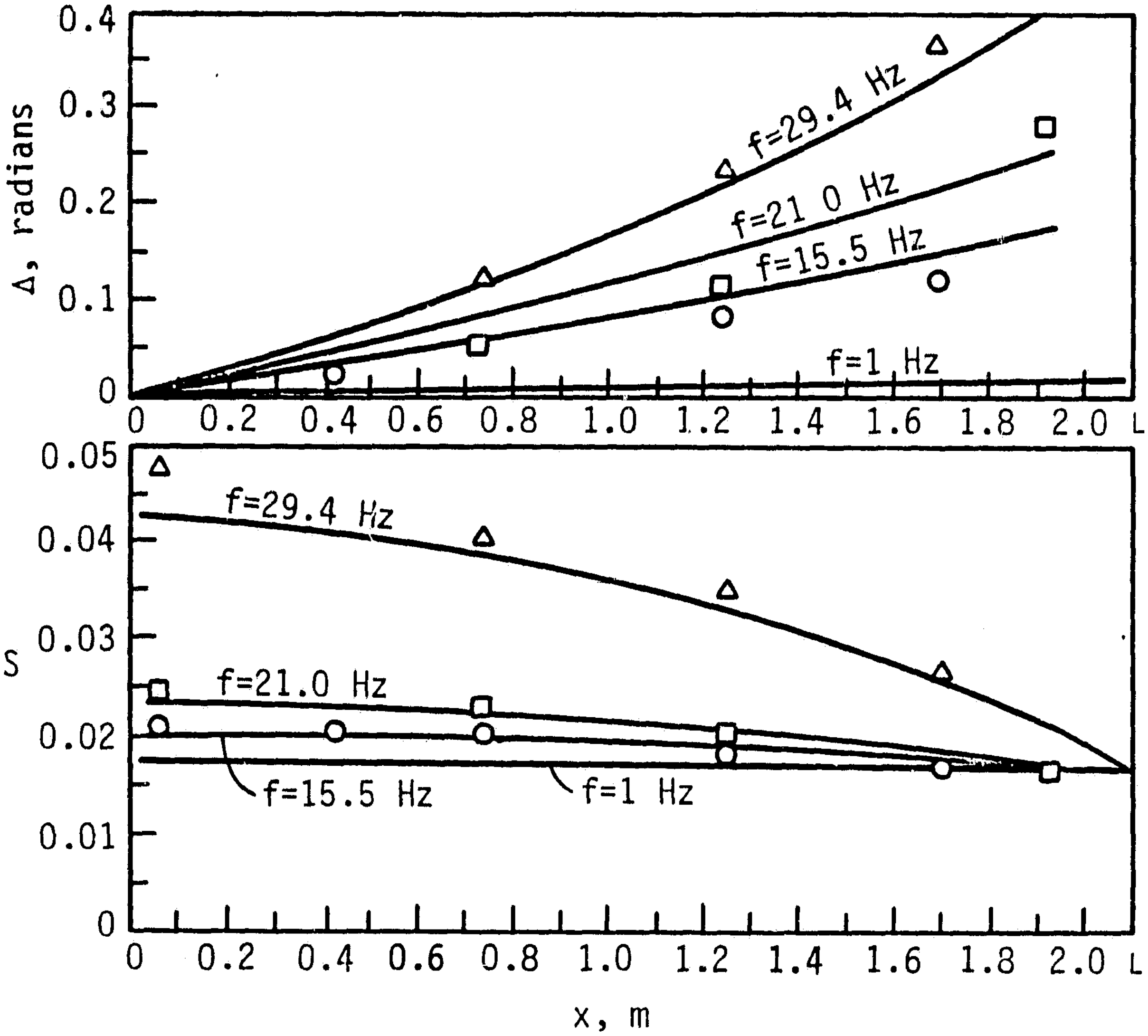

Figure 6. Comparison of measured and predicted variations in S and Δ. M_m = 0.142. Wedge stroke = 1.91 cm. ——— predictions; Experiment: ○, f = 15.5 Hz; □, f = 21.0 Hz; △, f = 29.4 Hz

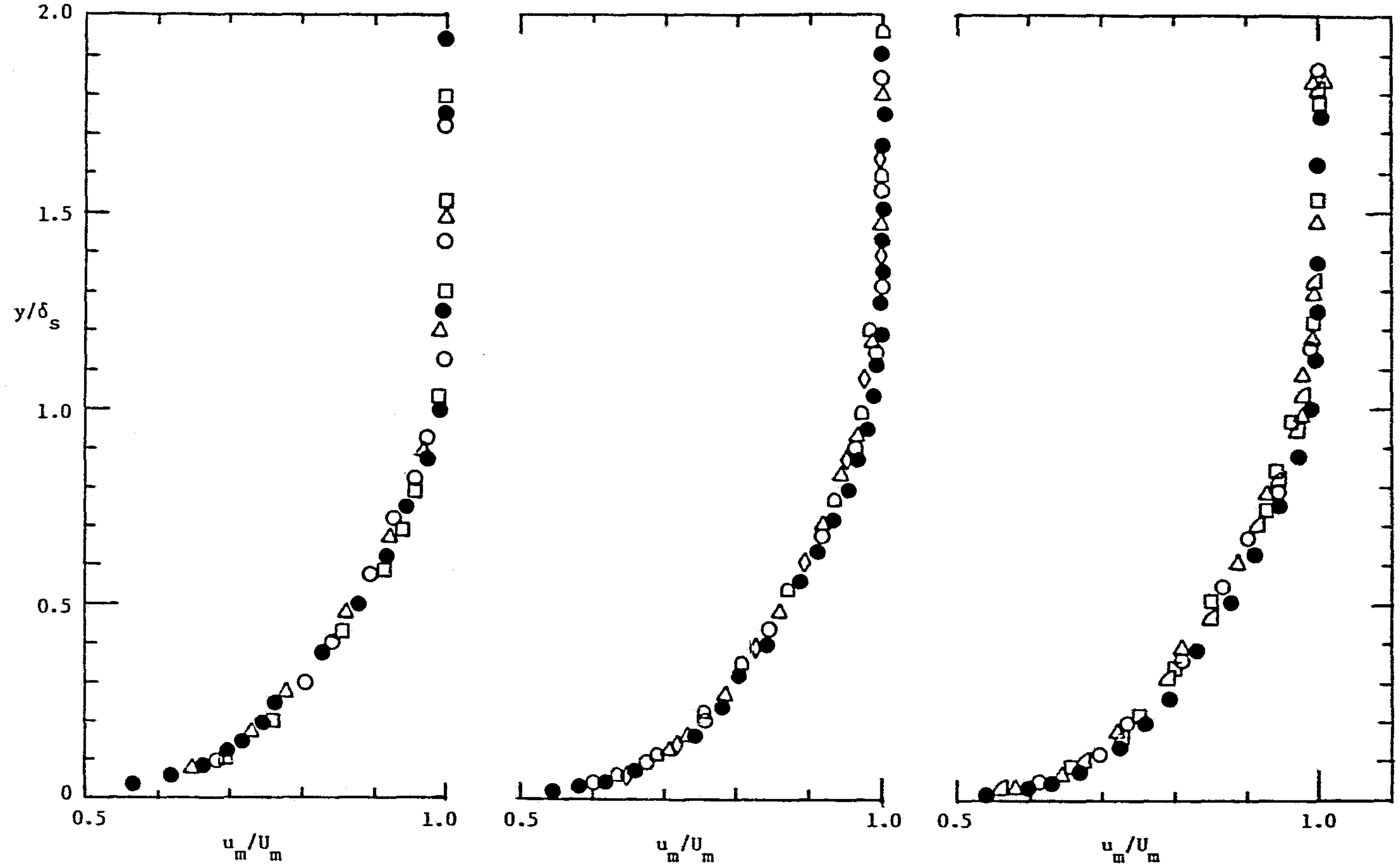

a. ξ = 0.61 m   b. ξ = 1.12 m   c. ξ = 1.58 m

Figure 7. Mean velocity profiles for oscillating flows measured at three values of ξ: ●, steady flow
a. ○, data set A1; □, data set A3; △, data set A4
b. ⌂, data set C1; ○, data set C2; △, data set C4; ◇, data set C6
c. ◁, data set D1; ○, data set D2; □, data set D4; △, data set D6

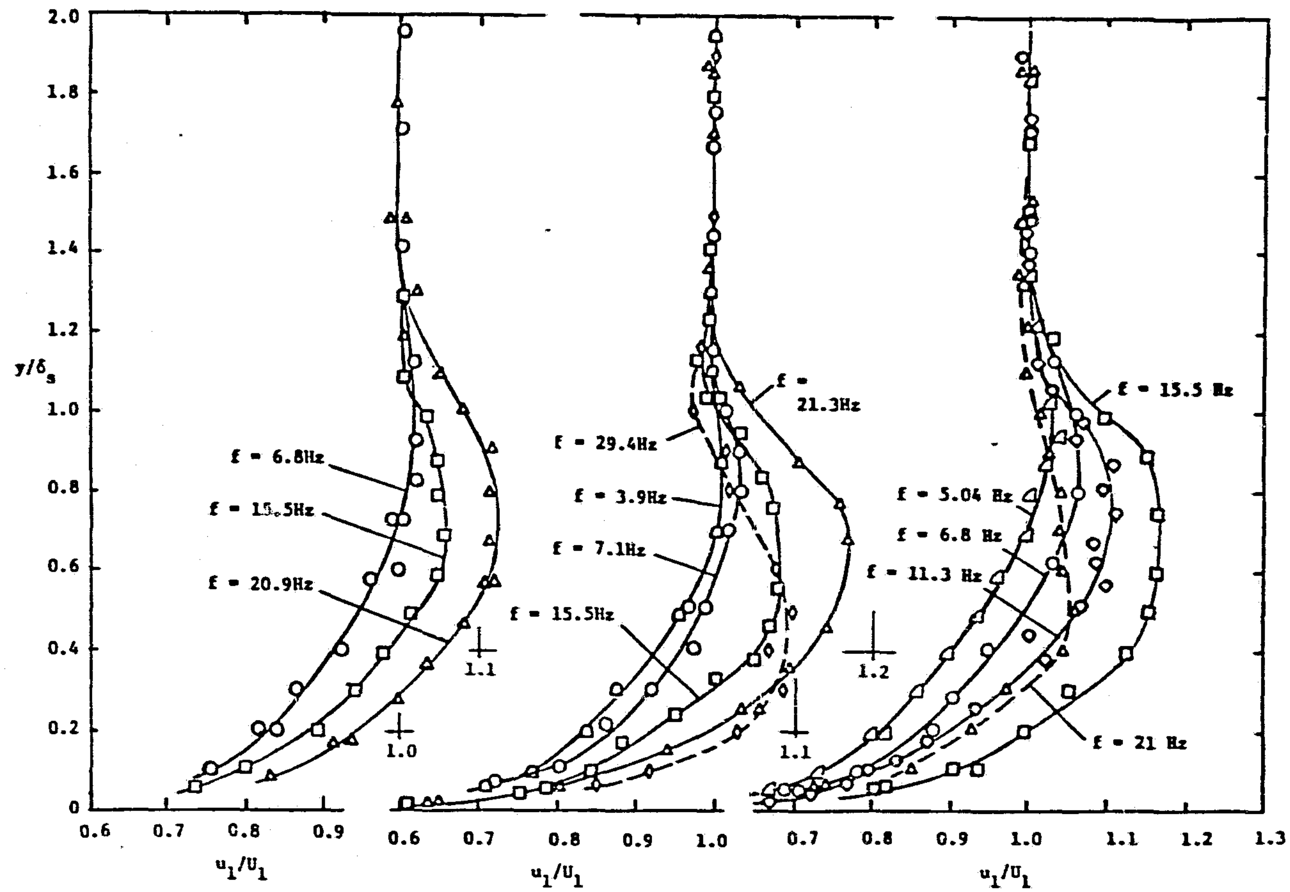

a. ξ = 0.61 m　　b. ξ = 1.12 m　　c. ξ = 1.58 m

Figure 8. Experimental profiles for u_1/U_1 at three ξ values and several frequencies. Wedge stroke = 1.91 cm.

a. ○, data set A1, $\bar{\omega}$ = 0.54; □, data set A3, $\bar{\omega}$ = 1.24; △, data set A4, $\bar{\omega}$ = 1.67.
b. ⌂, data set C1, $\bar{\omega}$ = 0.54; ○, data set C2, $\bar{\omega}$ = 1.0; □, data set C3, $\bar{\omega}$ = 2.19; △, data set C4, $\bar{\omega}$ = 3.01; ◇, data set C6, $\bar{\omega}$ = 4.16.
c. ◺, data set D1, $\bar{\omega}$ = 0.97; ○, data set D2, $\bar{\omega}$ = 1.31; ○, data set D3, $\bar{\omega}$ = 2.18; □, data set D4, $\bar{\omega}$ = 2.99; △, data set D6, $\bar{\omega}$ = 4.05.

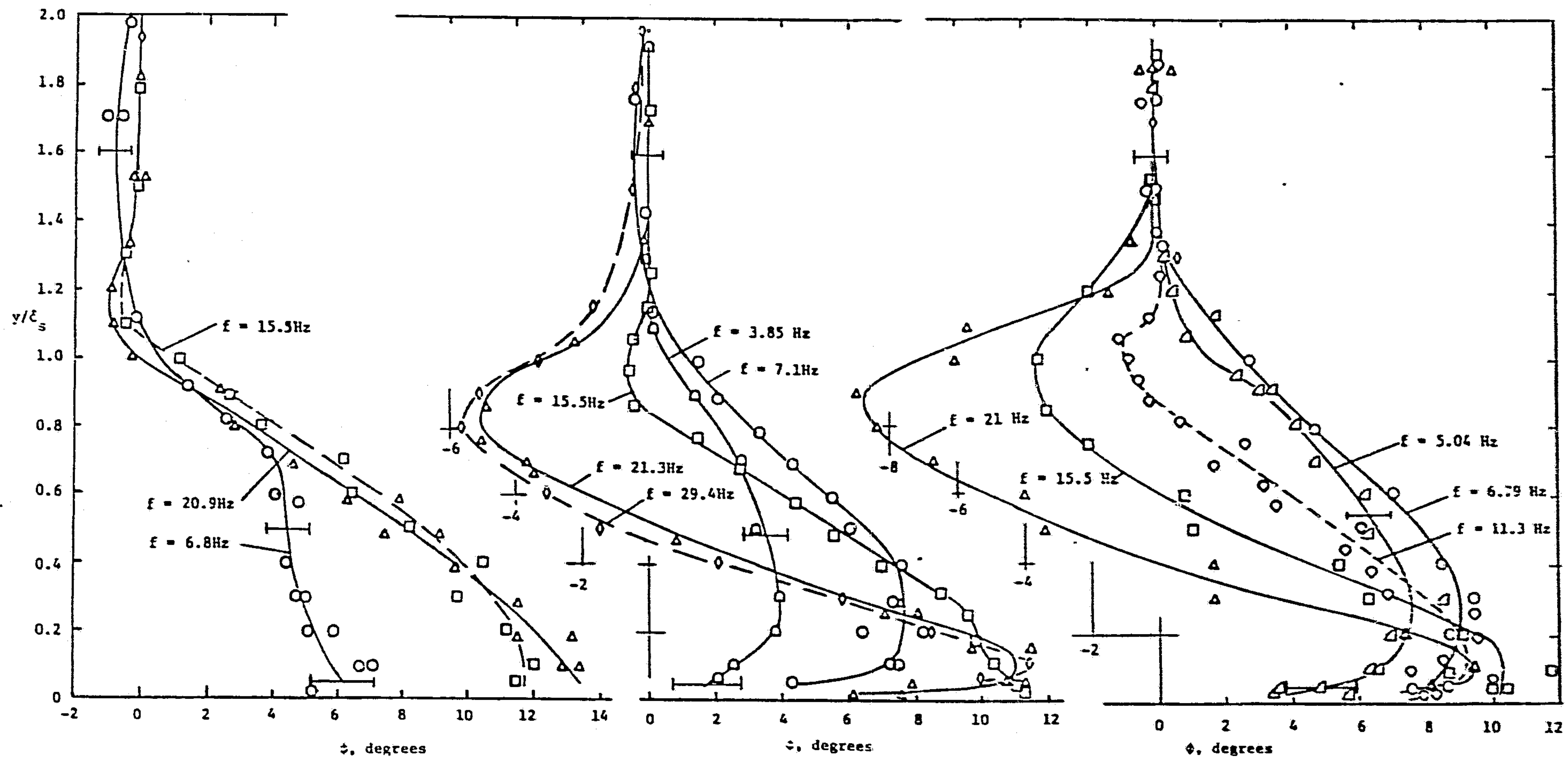

a. ξ = 0.61 m

b. ξ = 1.12 m

c. ξ = 1.58 m

Figure 9. Experimental profiles for ϕ at three ξ values and several frequencies. Wedge stroke = 1.91 cm.

a. ○, data set A1, $\bar{\omega} = 0.54$; □, data set A3, $\bar{\omega} = 1.24$; △, data set A4, $\bar{\omega} = 1.67$.

b. ◠, data set C1, $\bar{\omega} = 0.54$; ○, data set C2, $\bar{\omega} = 1.0$; □, data set C3, $\bar{\omega} = 2.19$; △, data set C4, $\bar{\omega} = 3.01$; ◊, data set C6, $\bar{\omega} = 4.16$.

c. ◿, data set D1, $\bar{\omega} = 0.97$; ○, data set D2, $\bar{\omega} = 1.31$; ◇, data set D3, $\bar{\omega} = 2.18$; □, data set D4, $\bar{\omega} = 2.99$; △, data set D6, $\bar{\omega} = 4.05$.

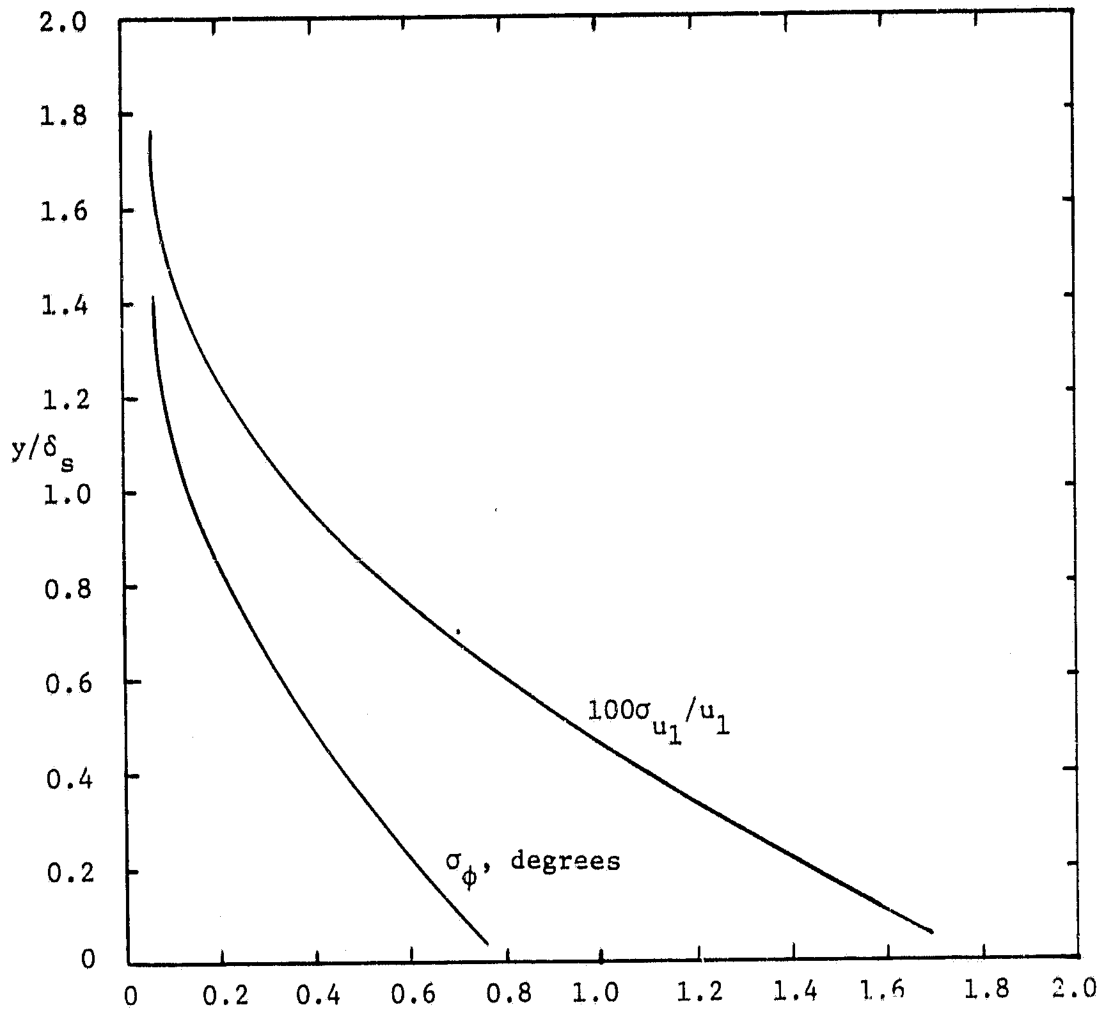

Figure 10. Estimated uncertainties in amplitude of oscillation and phase angle for velocity in oscillating flows. 210 cycles. Wedge stroke = 1.91 cm.

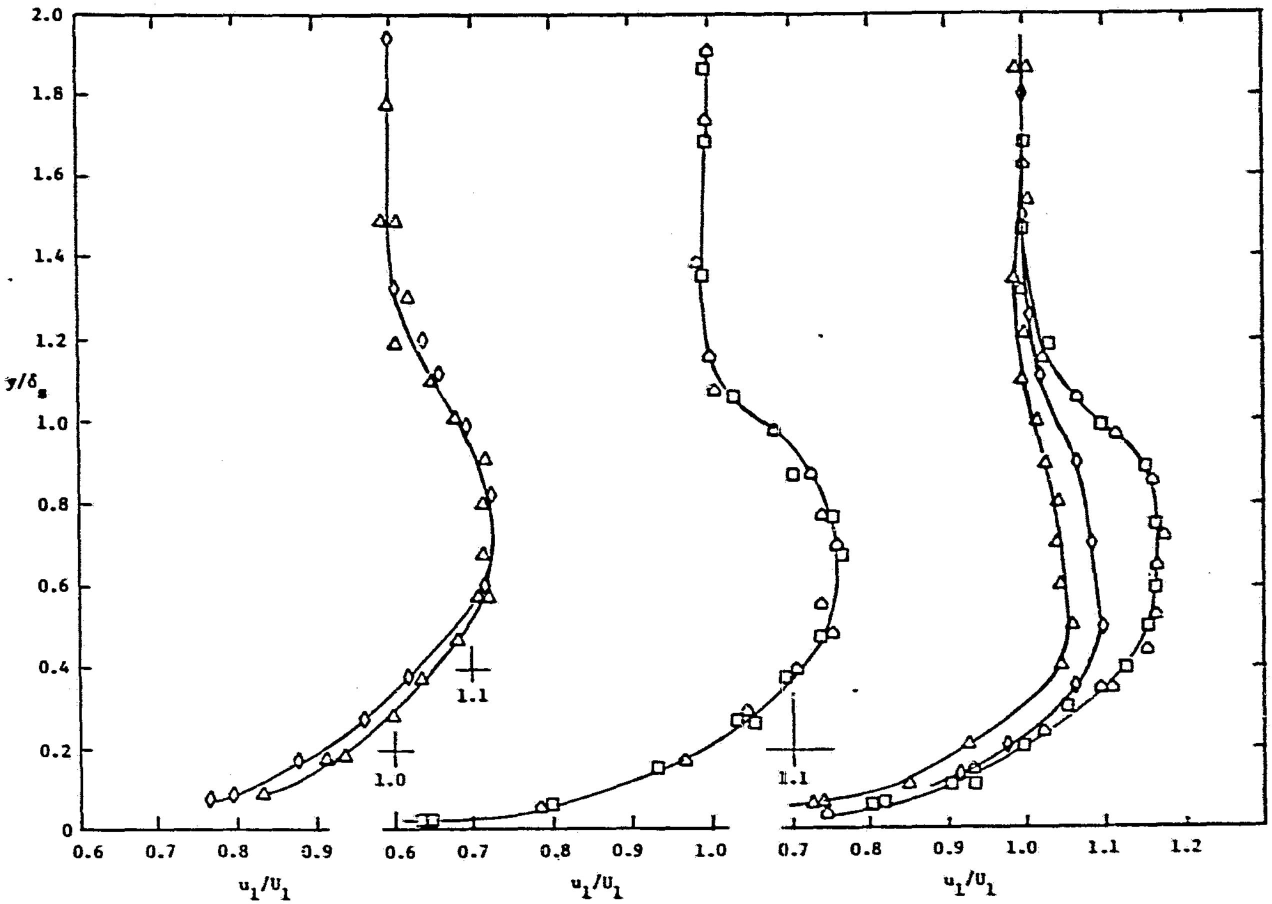

a. $\xi = 0.61$ m b. $\xi = 1.12$ m c. $\xi = 1.58$ m

Figure 11. Comparisons of experimental u_1/U_1 profiles for oscillating flows produced with different wedge strokes.

a. △, data set A4, $U_1/U_m = 0.169$, $f = 20.9$ Hz; ◊, data set A5, $U_1/U_m = 0.112$, $f = 20.9$ Hz

b. □, data set C4, $U_1/U_m = 0.152$, $f = 21.3$ Hz; ⌂, data set C5, $U_1/U_m = 0.097$, $f = 21.3$ Hz

c. □, data set D4, $U_i/U_m = 0.121$, $f = 15.5$ Hz; ⌂, data set D5, $U_1/U_m = 0.071$ $f = 15.1$ Hz; △, data set D6, $U_1/U_m = 0.136$, $f = 21.0$ Hz: ◊, D7, $U_1/U_m = 0.065$, $f = 21.0$ Hz

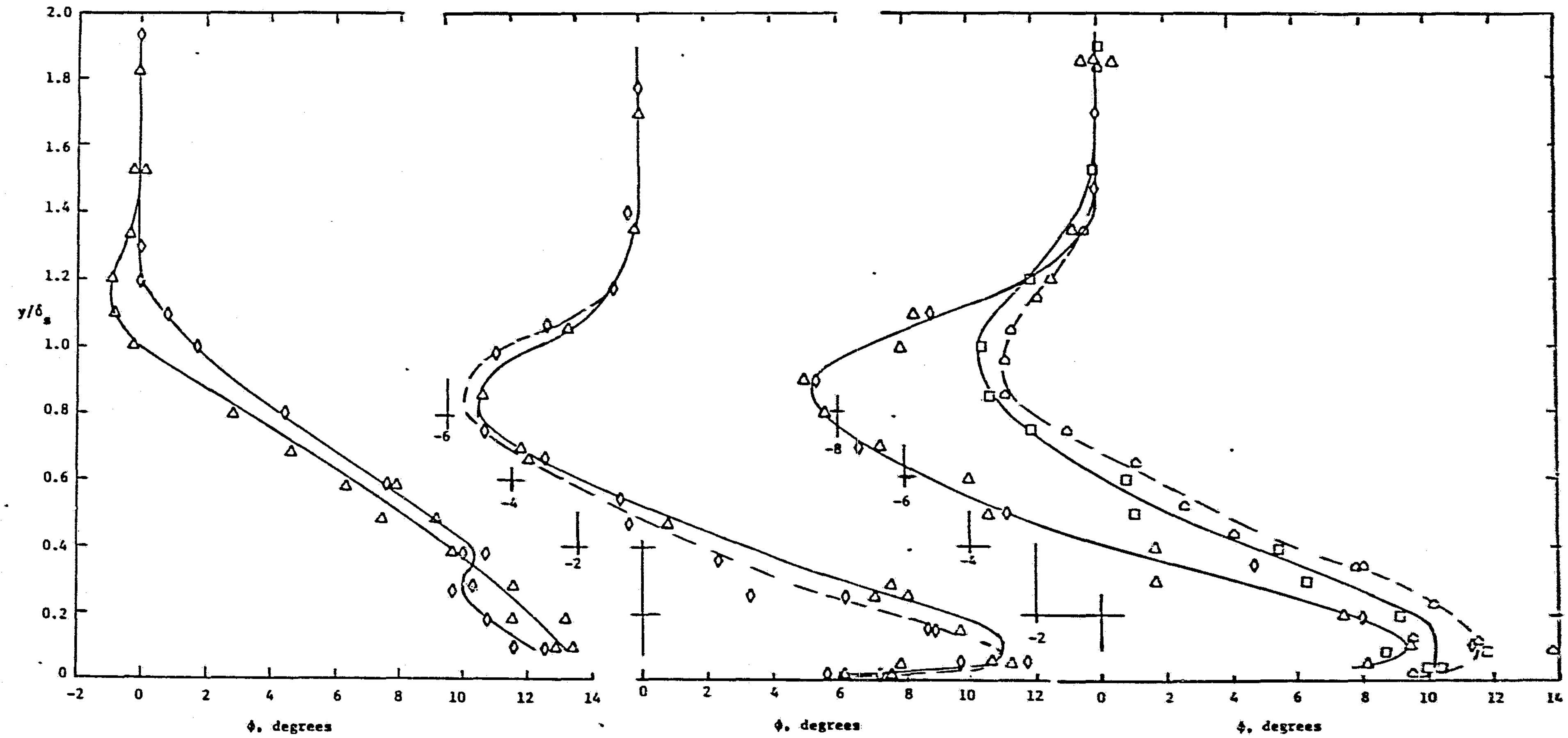

a. $\xi = 0.61$ m

b. $\xi = 1.12$ m

c. $\xi = 1.58$ m

Figure 12. Comparison of experimental ϕ profiles for oscillating flows produced with different wedge strokes.

a. △, data set A4, $U_1/U_m = 0.169$, $f = 20.9$ Hz; ◇, data set A5, $U_1/U_m = 0.112$, $f = 20.9$ Hz

b. □, data set C4, $U_1/U_m = 0.152$, $f = 21.3$ Hz; ⌂, data set C5, $U_1/U_m = 0.097$, $f = 21.3$ Hz

c. □, data set D4, $U_1/U_m = 0.121$, $f = 15.5$ Hz; ⌂, data set D5, $U_1/U_m = 0.071$ $f = 15.1$ Hz; △, data set D6, $U_1/U_m = 0.136$, $f = 21.0$ Hz: ◇, D7, $U_1/U_m = 0.065$, $f = 21.0$ Hz

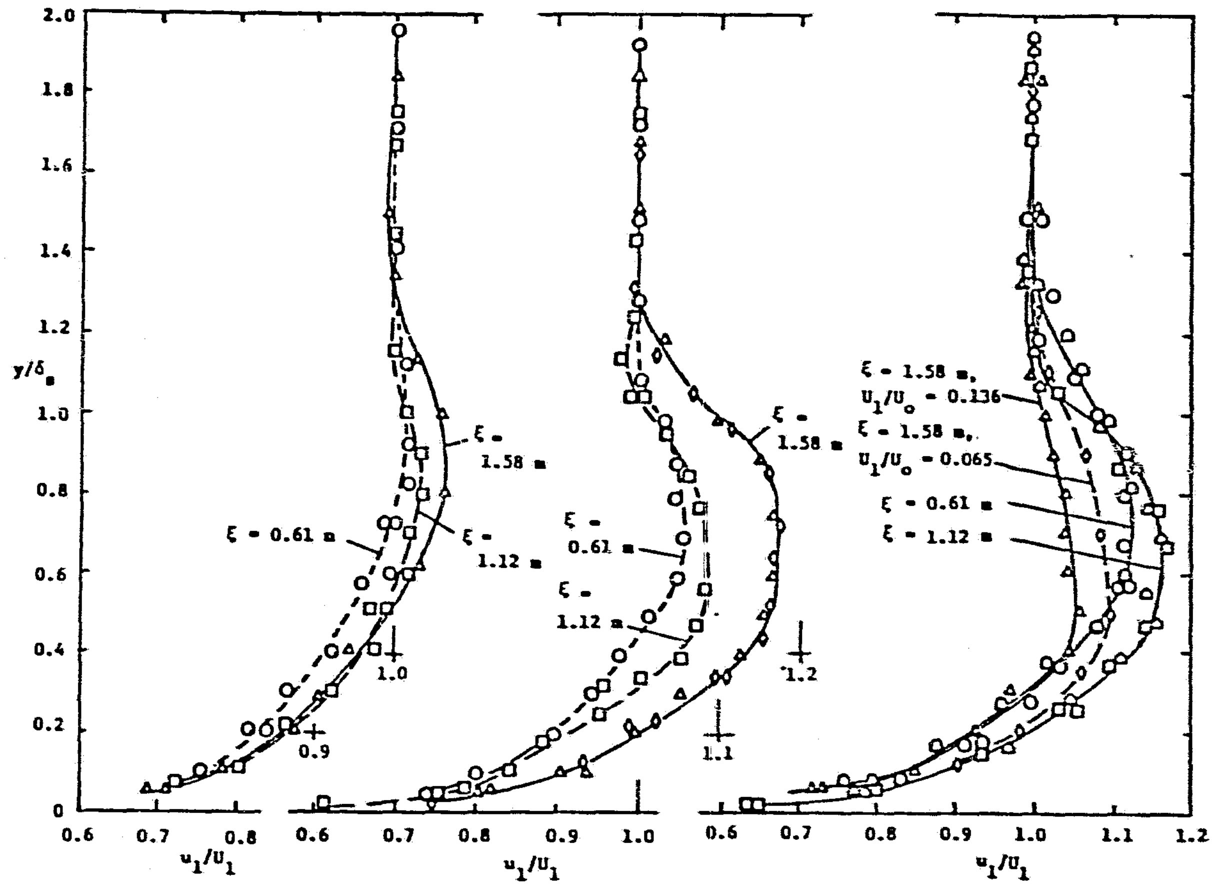

a. f = 7 Hz b. f = 15 Hz c. f = 21 Hz

Figure 13. Experimental u_1/U_1 profiles for three values of frequency.

a. ○, data set A1, f = 6.8 Hz; □, data set C1, f = 7.1 Hz; △, data set D2, f = 6.8 Hz

b. ○, data set A3, f = 15.5 Hz; □, data set C3, f = 15.5 Hz; △, data set D4, f = 15.5 Hz; ◇, data set D5, f = 15.1 Hz;

c. ○, data set A4, f = 20.9 Hz; ⌂, data set A5, f = 20.9 Hz; □, data set C4, f = 21.3 Hz; ⌂, data set C5, f = 21.3 Hz; △, data set D6, f = 21.0 Hz; ◇, data set D7, f = 21.0 Hz

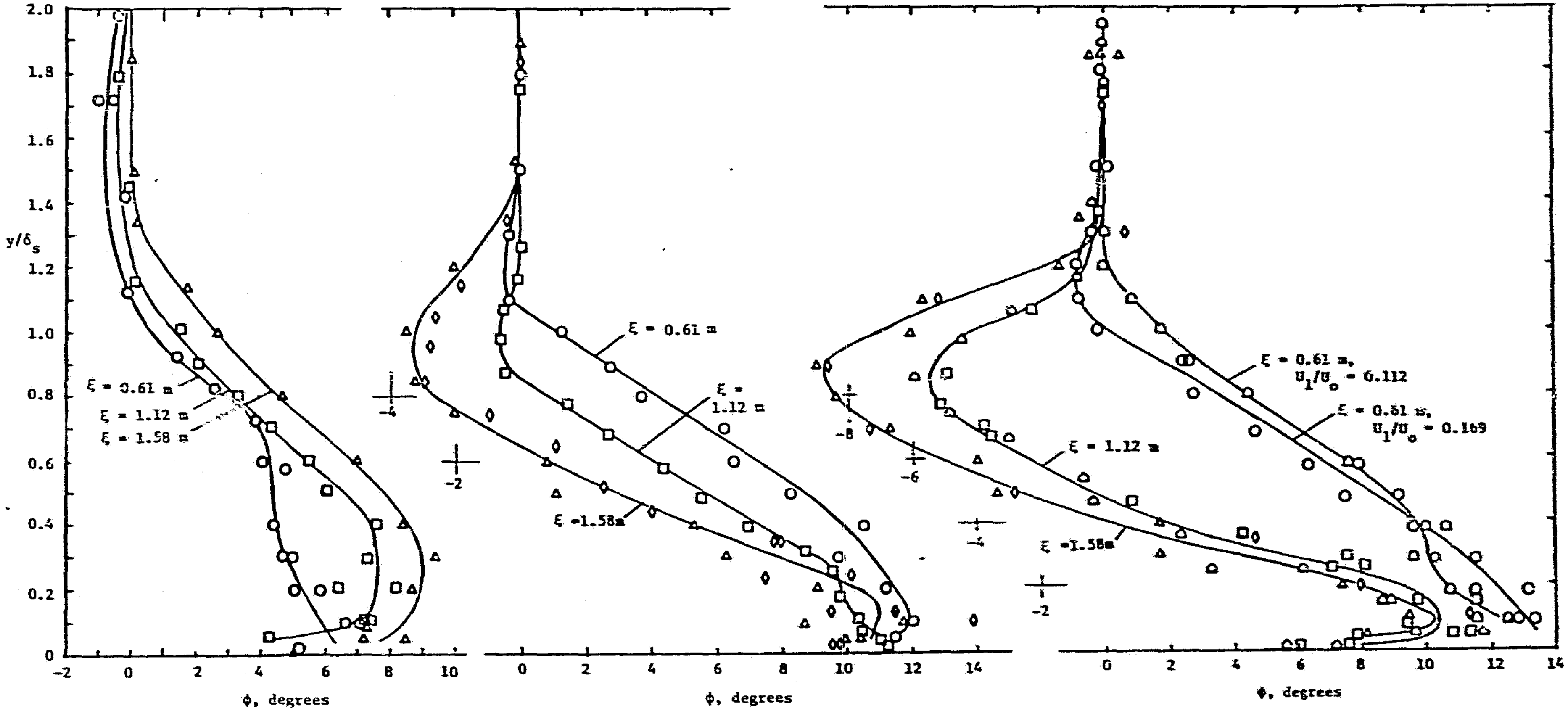

a. f = 7 Hz

b. f = 15 Hz

c. f = 21 Hz

Figure 14. Experimental ϕ profiles for three values of frequency.
a. ○, data set A1, f = 6.8 Hz; □, data set C1, f = 7.1 Hz; △, data set D2, f = 6.8 Hz
b. ○, data set A3, f = 15.5 Hz; □, data set C3, f = 15.5 Hz; △, data set D4, f = 15.5 Hz; ◊, data set D5, f = 15.1 Hz;
c. ○, data set A4, f = 20.9 Hz; ⌂, data set A5, f = 20.9 Hz; □, data set C4, f = 21.3 Hz; ⌂, data set C5, f = 21.3 Hz; △, data set D6, f = 21.0 Hz; ◊, data set D7, f = 21.0 Hz

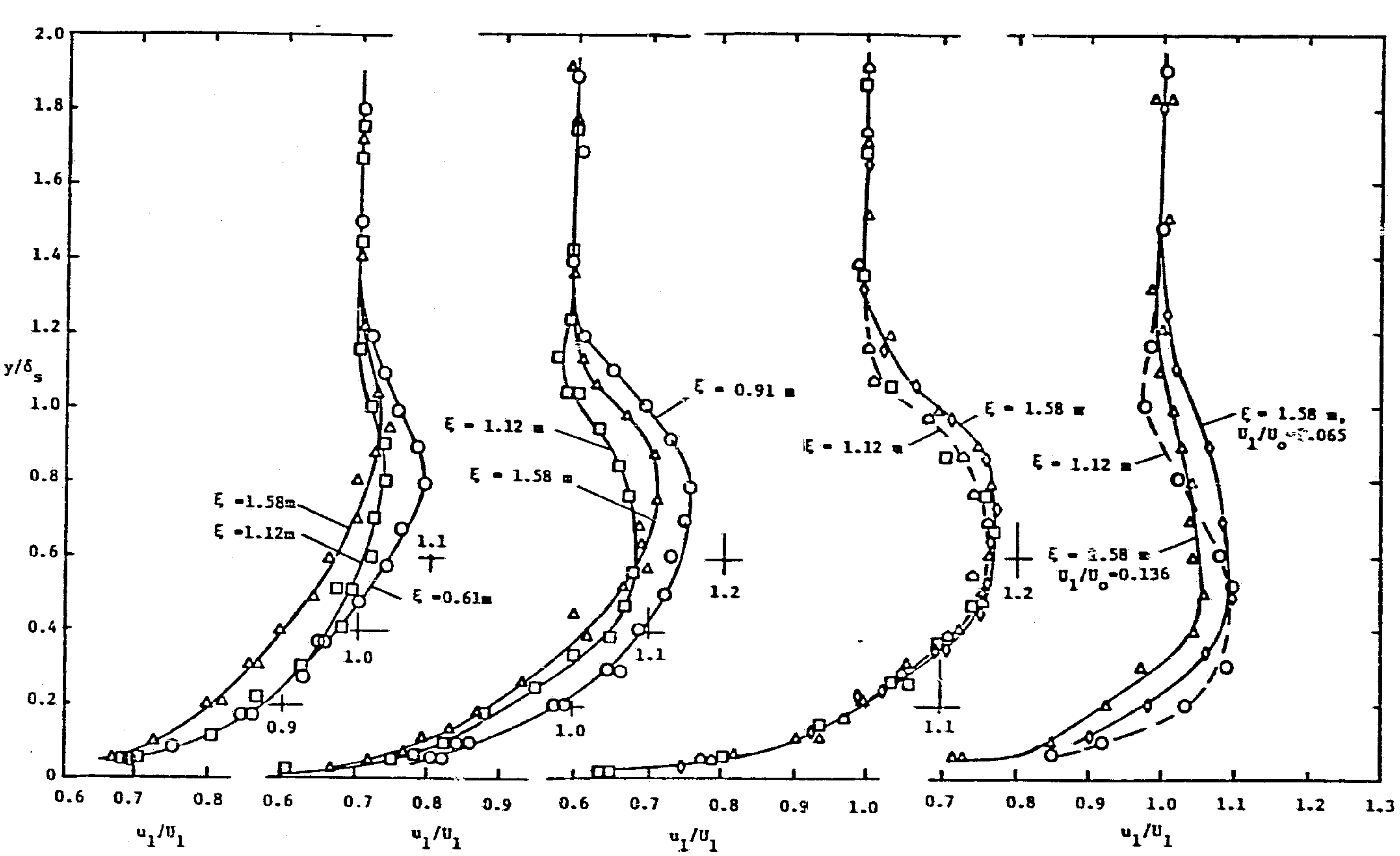

a. $\overline{\omega}$ = 1.0 b. $\overline{\omega}$ = 2.2 c. $\overline{\omega}$ = 3.0 d. $\overline{\omega}$ = 4.1

Figure 15. Experimental profiles for u_1/U_1 at four values of reduced frequency.

a. ○, data set A2, $\overline{\omega} = 1.04$; □, data set C2, $\overline{\omega} = 1.0$; △, data set D1, $\overline{\omega} = 0.97$

b. ○, data set B1, $\overline{\omega} = 2.24$; □, data set C3, $\overline{\omega} = 2.19$; △, data set D3, $\overline{\omega} = 2.18$

c. □, data set C4, $\overline{\omega} = 3.01$; ⌂, data set C5, $\overline{\omega} = 3.01$; △, data set D4, $\overline{\omega} = 2.99$; ◊, data set D5, $\overline{\omega} = 2.91$

d. ○, data set C6, $\overline{\omega} = 4.16$; △, data set D6, $\overline{\omega} = 4.05$; ◊, data set D7, $\overline{\omega} = 4.05$

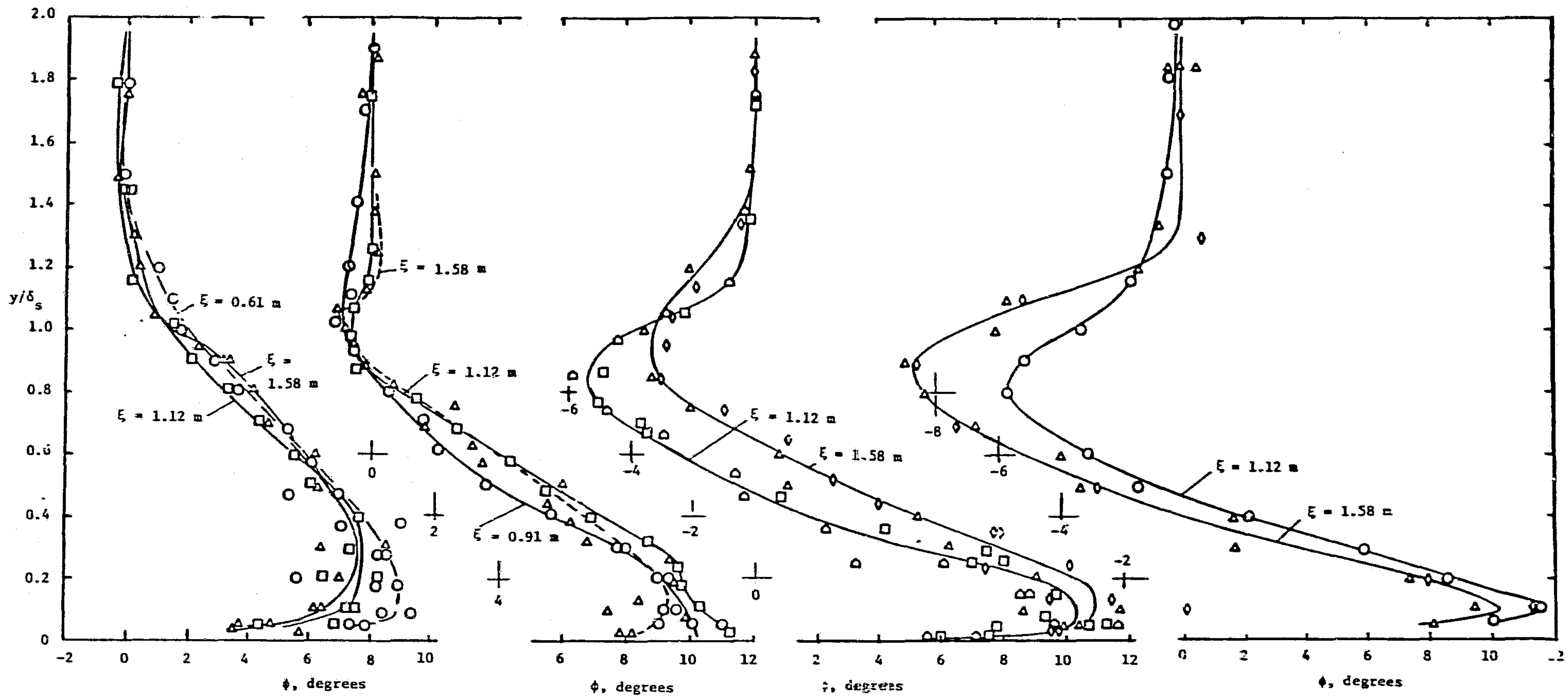

a. $\overline{\omega}$ = 1.0   b. $\overline{\omega}$ = 2.2   c. $\overline{\omega}$ = 3.0   d. $\overline{\omega}$ = 4.1

Figure 16. Experimental profiles for ϕ at four values of reduced frequency.
a. ○, data set A2, $\bar{\omega}$ = 1.04; □, data set C2, $\bar{\omega}$ = 1.0;
△, data set D1, $\bar{\omega}$ = 0.97
b. ○, data set B1, $\bar{\omega}$ = 2.24; □, data set C3, $\bar{\omega}$ = 2.19;
△, data set D3, $\bar{\omega}$ = 2.18
c. □, data set C4, $\bar{\omega}$ = 3.01; ⌂, data set C5, $\bar{\omega}$ = 3.01;
△, data set D4, $\bar{\omega}$ = 2.99; ◊, data set D5, $\bar{\omega}$ = 2.91
d. ○, data set C6, $\bar{\omega}$ = 4.16; △, data set D6, $\bar{\omega}$ = 4.05;
◊, data set D7, $\bar{\omega}$ = 4.05

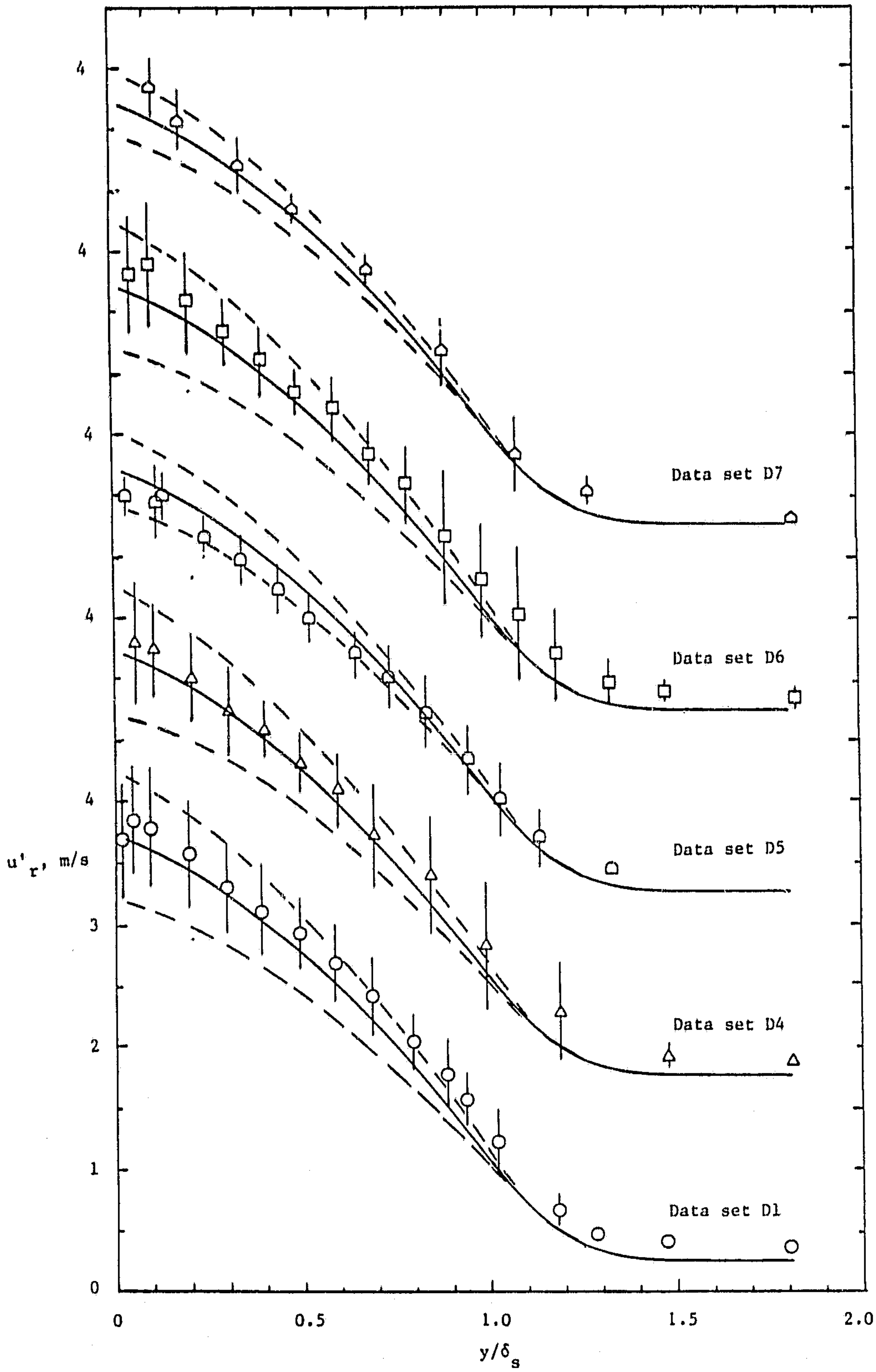

Figure 17. Comparisons of mean values and amplitudes for u'_r. ξ = 1.58 m. Quasi-steady flows: ——— u'_{rm}; — — — $u'_{rm} \pm u'_{r1}$ Experiment: ○, data set D1, f = 5.04 Hz, U_1/U_m = 0.126; △, data set D4, f = 15.5 Hz, U_1/U_m = 0.121; ⌓, data set D5, f = 15.5 Hz, U_1/U_m = 0.071; □, data set D6, f = 21.0 Hz, U_1/U_m = 0.136; ⌂, data set D7, f = 21.0 Hz, U_1/U_m = 0.065. Vertical lines indicate range of u'_r.

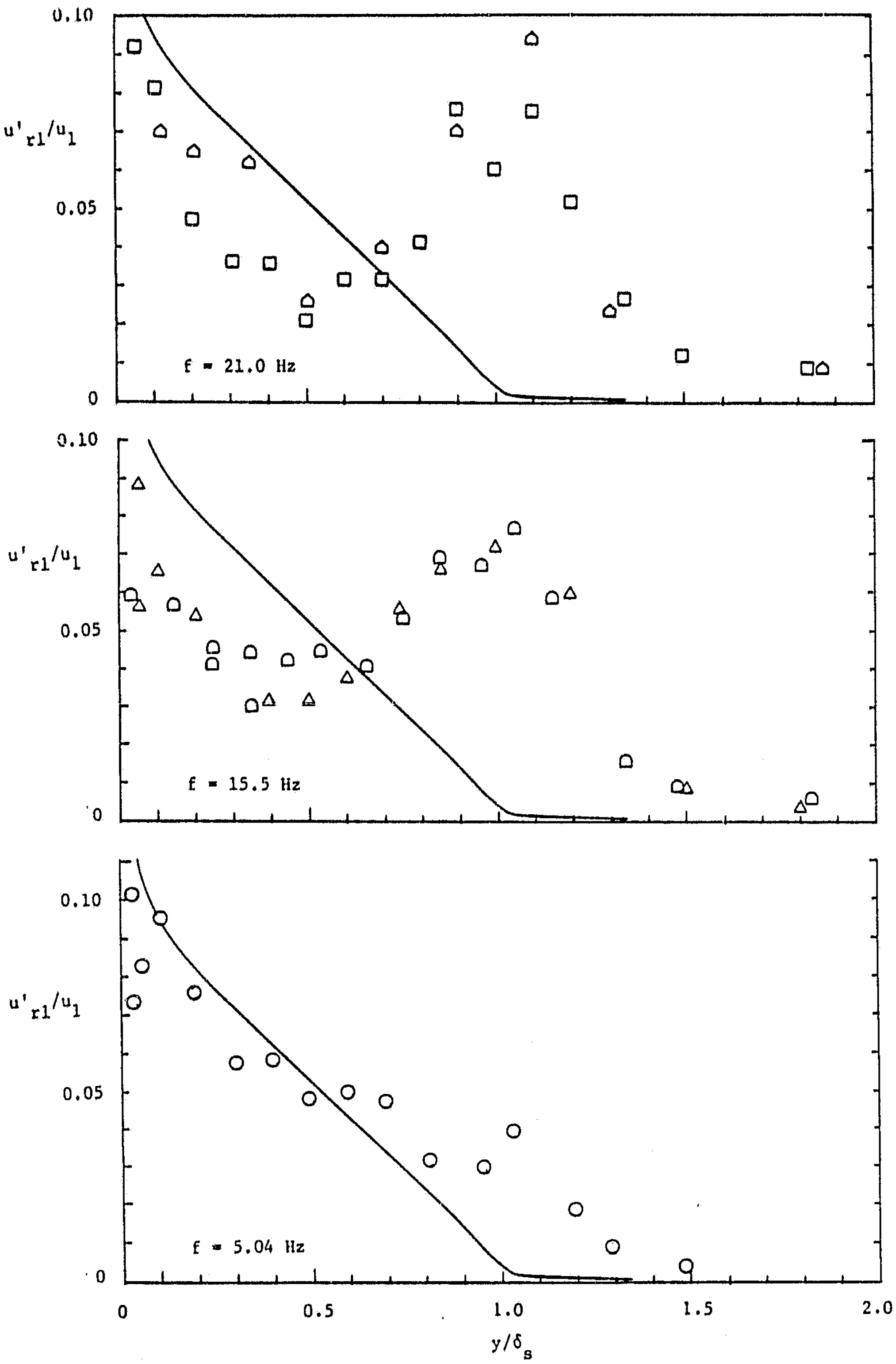

Figure 18. Results for u'_{r1}/u_1 vs y/δ_s at ξ = 1.58 m.
Quasi steady flow: ———————
Experiment: ○, data set D1, f = 5.04 Hz, U_1/U_m = 0.126; △, data set D4, f = 15.5 Hz, U_1/U_m = 0.121; ⌂, data set D5, f = 15.5 Hz, U_1/U_m = 0.071; □, data set D6, f = 21.0 Hz, U_1/U_m = 0.136; ⌂, data set D7, f = 21.0 Hz, U_1/U_m = 0.065.

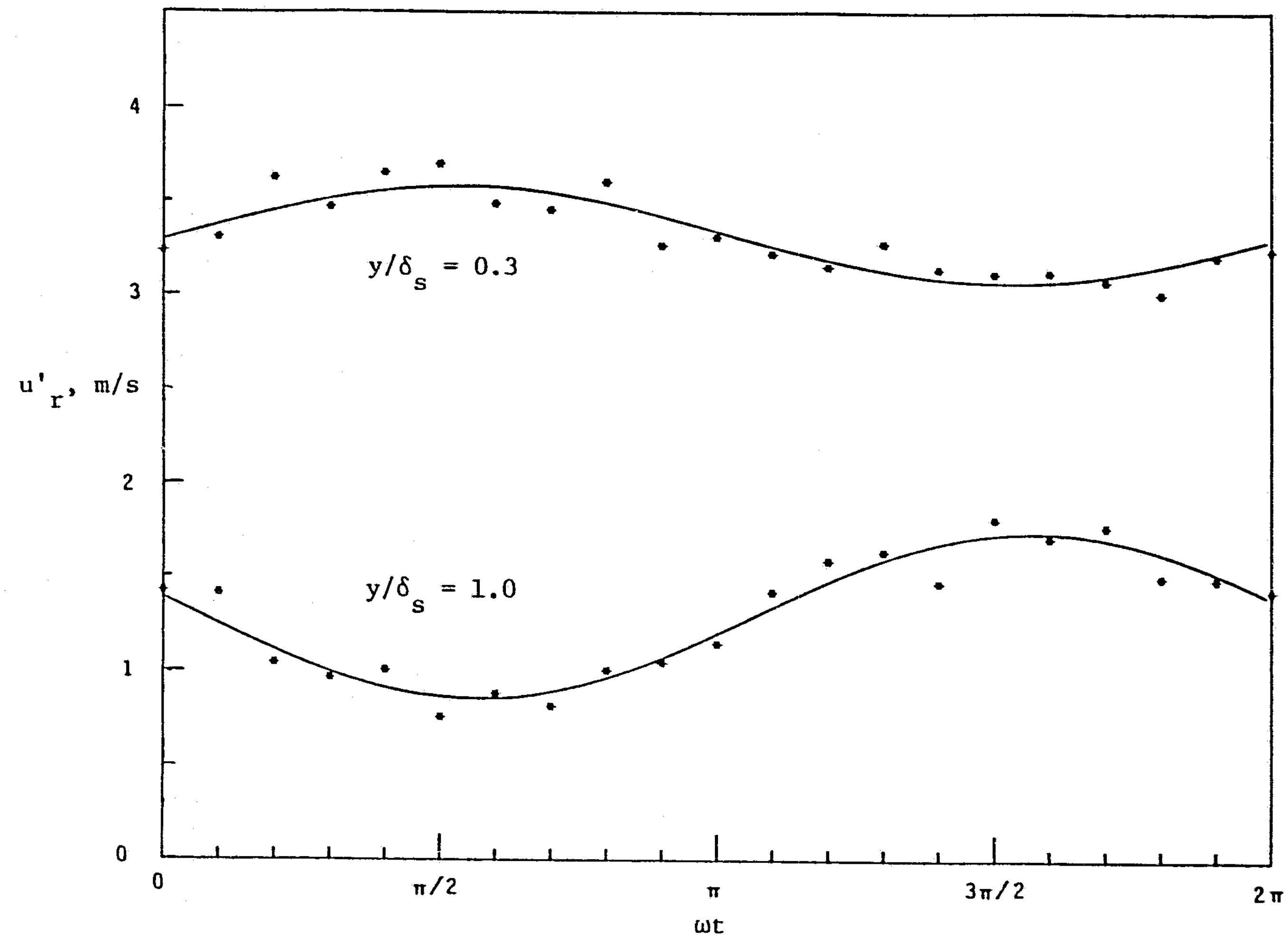

Figure 19. Experimental variations in u'_r from data set D6. $\xi = 1.58$ m. *, ensemble averaged velocity, 210 cycles;—— fitted cosine curve.

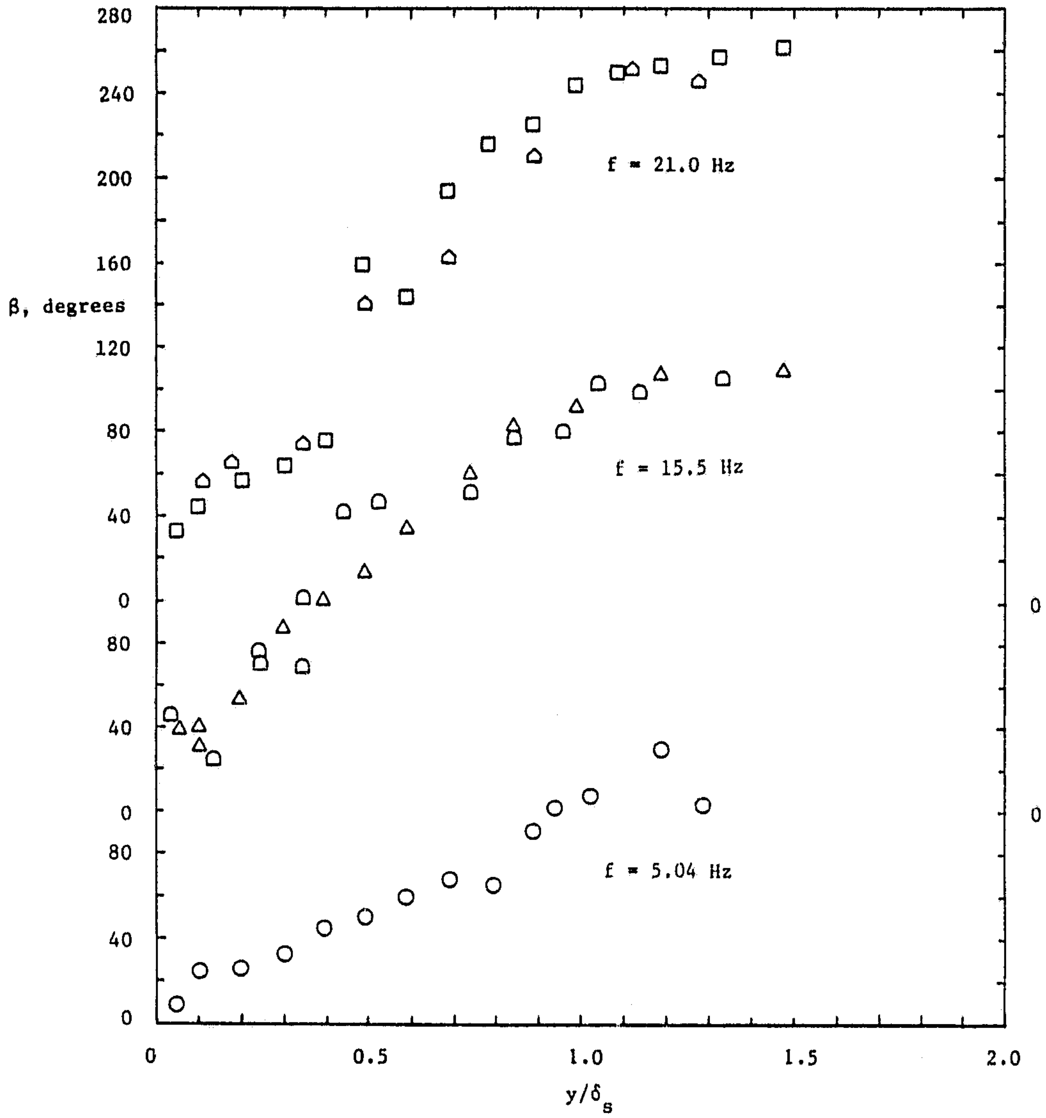

Figure 20. Variation in β, the angle by which u'_r lags the local boundary layer velocity u, with y/δ_s. ξ = 1.58 m. Experiment: ○, data set D1, f = 5.04 Hz, U_1/U_m = 0.126; △, data set D4, f = 15.5 Hz, U_1/U_m = 0.121; ⌓, data set D5, f = 15.5 Hz, U_1/U_m = 0.071; □, data set D6, f = 21.0 Hz, U_1/U_m = 0.136; ⌂, data set D7, f = 21.0 Hz, U_1/U_m = 0.065.

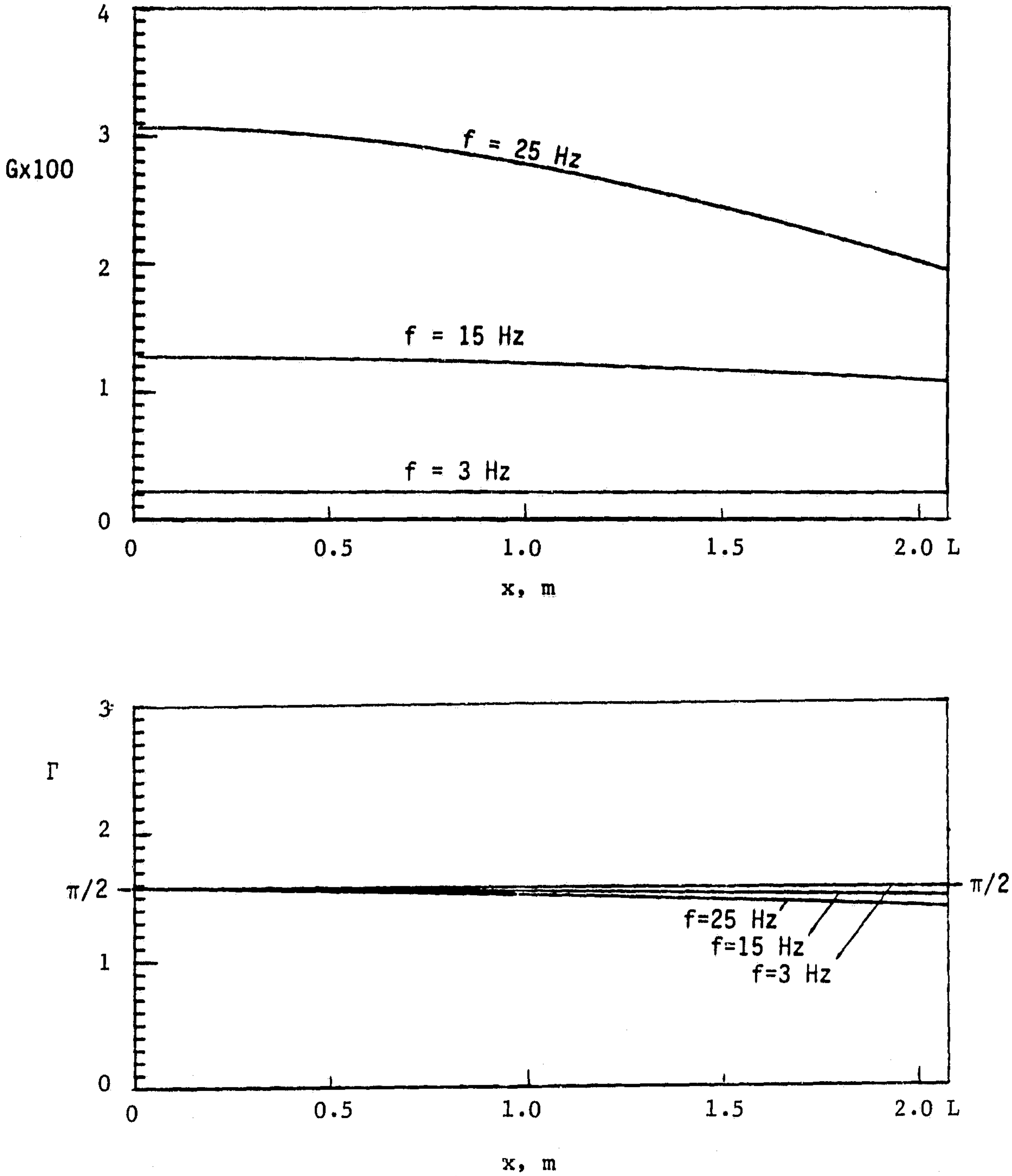

Figure 21. G and Γ, equation (6.8), vs x at three values of frequency for flows in the present facility. Wedge stroke = 1.91 cm.

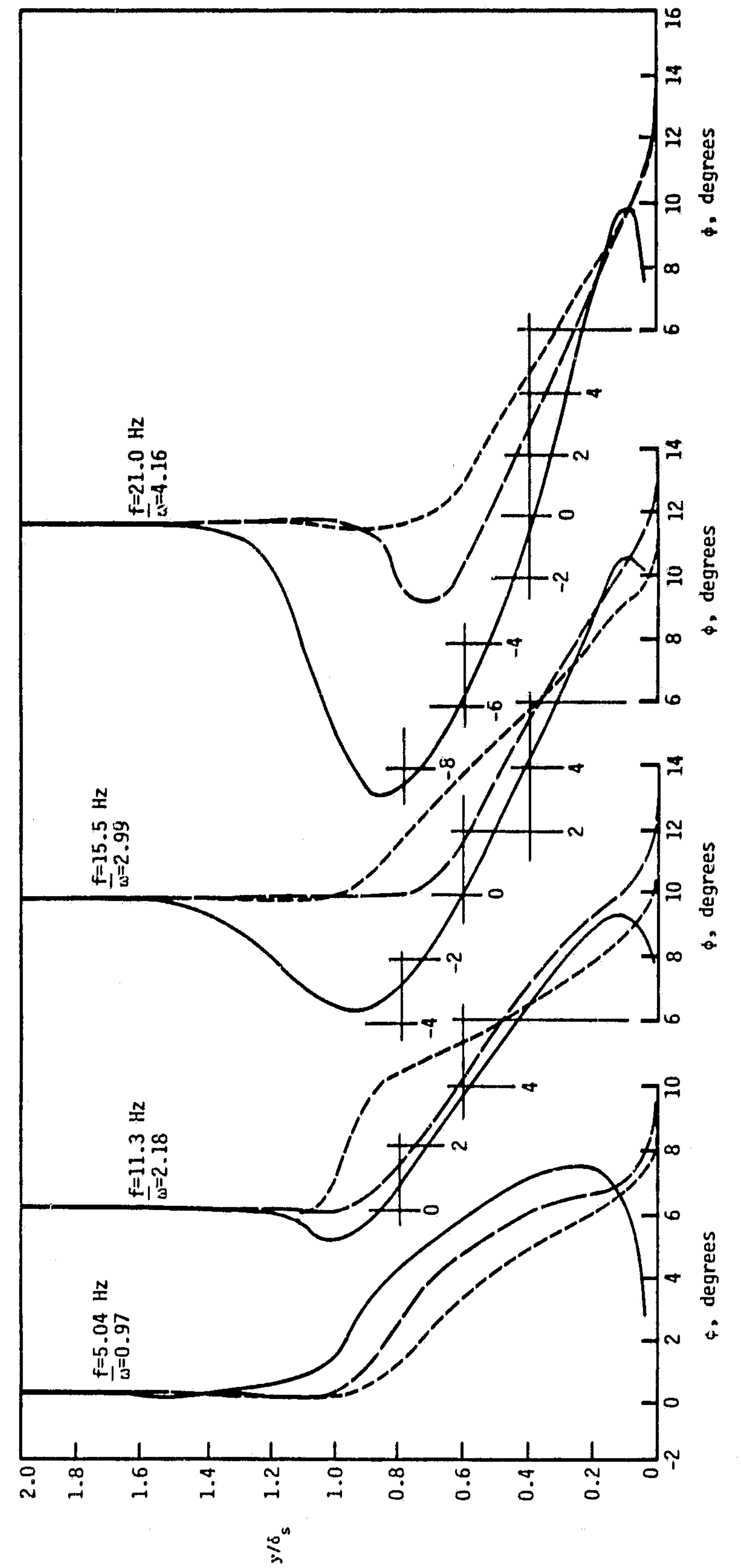

c.

Figure 22. Concluded